HAL open science

Successes, challenges, and opportunities for quantum chemistry in understanding metalloenzymes for solar fuels research

Maylis Orio, Dimitrios A Pantazis

To cite this version:

Maylis Orio, Dimitrios A Pantazis. Successes, challenges, and opportunities for quantum chemistry in understanding metalloenzymes for solar fuels research. Chemical Communications, 2021, 57 (33), pp.3952-3974. 10.1039/d1cc00705j . hal-03411777

HAL Id: hal-03411777

https://hal.science/hal-03411777v1

Submitted on 2 Nov 2021

HAL is a multi-disciplinary open access archive for the deposit and dissemination of scientific research documents, whether they are published or not. The documents may come from teaching and research institutions in France or abroad, or from public or private research centers.

L'archive ouverte pluridisciplinaire **HAL**, est destinée au dépôt et à la diffusion de documents scientifiques de niveau recherche, publiés ou non, émanant des établissements d'enseignement et de recherche français ou étrangers, des laboratoires publics ou privés.

Distributed under a Creative Commons Attribution 4.0 International License

Please do not adjust margins

FEATURE ARTICLE

Successes, challenges, and opportunities for quantum chemistry in understanding metalloenzymes for solar fuels research

Received 00th January 20xx,
Accepted 00th January 20xx

DOI: 10.1039/x0xx00000x

Maylis Orio[a] and Dimitrios A. Pantazis[b]

Quantum chemical approaches today are a powerful tool to study the properties and reactivity of metalloenzymes. In the field of solar fuels research these involve predominantly photosystem II and hydrogenases, which catalyze water oxidation and hydrogen evolution, as well as related biomimetic and bio-inspired models. Theoretical methods are extensively used to better comprehend the nature of catalytic intermediates, establish important structure–function and structure–property correlations, elucidate functional principles, and uncover the catalytic activity of these complex systems by unravelling the key steps of their reaction mechanism. Computations in the field of water oxidation and hydrogen evolution are used as predictive tools to elucidate structures, explain and synthesize complex experimental observations from advanced spectroscopic techniques, rationalize reactivity on the basis of atomistic models and electronic structure, and guide the design of new synthetic targets. This feature article covers recent advances in the application of quantum chemical methods for understanding the nature of catalytic intermediates and the mechanism by which photosystem II and hydrogenases achieve their function, and points at essential questions that remain only partly answered and at challenges that will have to be met by future advances and applications of quantum and computational chemistry.

1. Introduction

The pressing need to develop energy sources and alternative fuels that are based on renewable, environmentally friendly, and affordable approaches is critical for successfully facing the mounting energy and climate challenges.[1, 2] Molecular solar fuels, such as hydrogen,[3] that can in principle be obtained by mimicking biological processes, represent the most promising way of meeting this need. In the hydrogen evolution reaction (HER), electrons and protons are combined to generate molecular H_2, which stores energy in its chemical bond. Hydrogen production through water splitting is one of the preferred solutions in the long run for the storage of renewable energy. Today hydrogen is principally used for industrial processes. However, it has the potential to play a major role as energy carrier in transportation, the gas industry, as well as in the generation of electricity and heat. In addition to other technical challenges, for the expansion of H_2 usage in these directions it would be necessary to increase the global production of H_2 considerably and sustainably.[4]

[a] Aix-Marseille Université, CNRS, iSm2, Marseille, France.
[b] Max-Planck-Institut für Kohlenforschung, Kaiser-Wilhelm-Platz 1, 45470 Mülheim an der Ruhr, Germany

Nature can provide useful guidelines in this quest, because metalloenzymes involved in water oxidation and hydrogen evolution serve as archetypes for these reactions and for the development of artificial catalysts for solar fuels.[2, 5-14] Nature offers a unique example of a water-oxidizing enzyme, photosystem II (PSII).[15, 16] This harbours the oxygen-evolving complex (OEC) with its manganese–calcium cluster (Scheme 1a) that catalyses the oxidation of water into dioxygen, protons, and electrons, powered by light-driven charge separation. Several aspects of the function of PSII remain unclear,[17] while the development of molecular manganese-based structural mimics of the OEC[18-25] has not been accompanied by comparable catalytic water oxidizing activity.[26-28]

In terms of H_2 evolution, biology provides good examples in hydrogenases (HG). These enzymes contain nickel and iron active sites (Scheme 1b) and achieve catalytic performances that rival synthetic platinum-based catalysts for hydrogen production.[29-32] Therefore, in analogy to the manganese-based water oxidizing PSII, hydrogenases serve to inspire the design of artificial hydrogen evolution catalysts based on Earth-abundant metals.[33] Several studies have reported homo-[34-37] and hetero-polynuclear[38-41] metal complexes as electrocatalysts for HER reproducing the structure of the active site of hydrogenases. In addition to biomimetic approaches, a variety of molecular electrocatalysts have been developed to facilitate hydrogen production by making it occur faster with a lower energy input. Up to now, platinum-based

Please do not adjust margins

Please do not adjust margins

catalysts provide the best performance in hydrogen evolution.[42] However, due to its scarcity and cost, intense research efforts have been devoted in developing non-noble transition metal catalysts.[43] In this connection, diverse ligand skeletons with cobalt, iron, and nickel complexes[44-51] were shown to evolve hydrogen both in organic and aqueous media (Scheme 2).

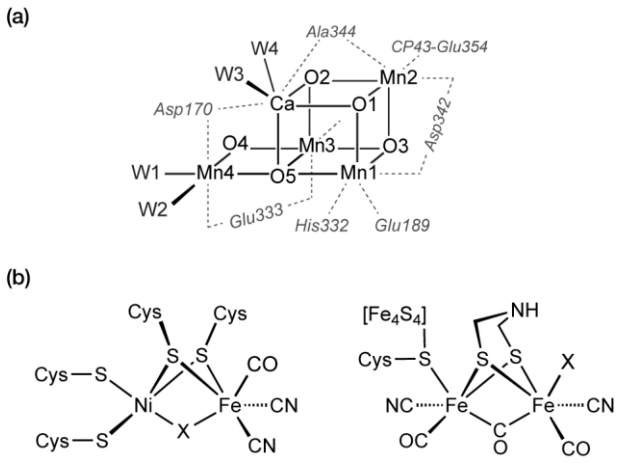

Scheme 1. (a) Structure of the Mn_4CaO_5 cluster in the active site of the OEC of photosystem II, showing standard atom labelling. W1–W4 represent water-derived ligands. (b) Structures of the active sites of the [NiFe] and [FeFe] hydrogenases, with X representing the site for catalytic H_2/proton turnover.

Research in the PSII and HG fields has benefited greatly from the contributions of quantum chemistry. During the last two decades of the 20th century the density functional theory (DFT) revolution extended the applicability of quantum chemistry to realistic transition metal systems in general and metalloenzymes in particular.[52-56] Particularly after the advent of hybrid functionals it was possible to predict molecular structures and reaction profiles with sufficient accuracy to make meaningful analysis of geometric and mechanistic aspects of bioinorganic systems. The further combination of DFT with classical force-field methods within QM/MM approaches[57] has become a considerably powerful component of modern computational chemistry.

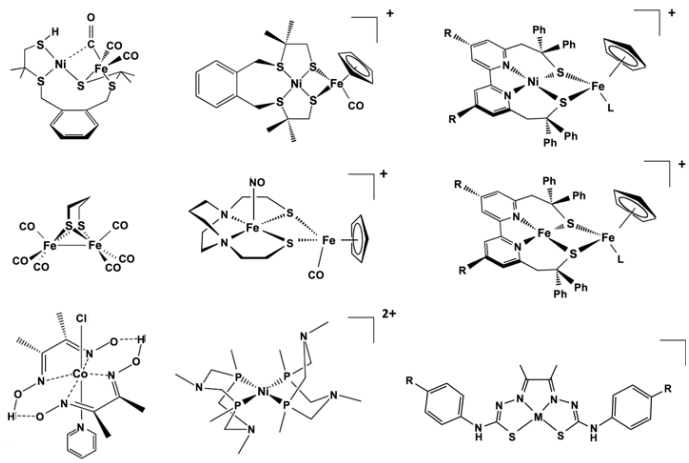

Scheme 2. Selected biomimetic and bioinspired models of the hydrogenases.[39, 40, 44, 45, 58-63]

The first two decades of the 21st century broadened even more the realm of applicability of quantum chemistry to metalloenzymes. One major development is that "quantum chemistry" in this field is no longer synonymous with "DFT", but relentless advances in methodology, implementation, and infrastructure have made single and multireference wave function theory a practical and accessible option. Moreover, quantum chemistry today reaches much further than mere geometry optimizations and simple reaction energetics. Theoretical advances mean that much deeper insights into the electronic structure and properties can be obtained, and hence much deeper and more insightful connections with experiment can be established.

The two title systems of the present feature article, photosystem II and hydrogenases, have served as application platforms on which quantum chemistry has reached new heights in terms of what can be computed, and how it advances the broader research fields. In the following we will describe selected examples of specific challenges that have been met for each system using quantum chemistry, focusing on properties and questions that require more than a trivial application of standard computational approaches. Furthermore, we will point to challenges that remain to be satisfactorily addressed, and to opportunities for future theoretical advances and demanding applications. Thus, we hope to offer a broad overview of where we stand and to provide motivation towards expanding the frontiers of quantum chemistry as applied to these metalloenzymes.

2. Photosystem II

Photosynthesis involves light harvesting, excitation energy transfer, and creation of charge separated states that drive subsequent redox transformations.[15, 16] In oxygenic photosynthesis the pigment–protein complex PSII utilizes this charge separation, likely initiated at the primary donor Chl_{D1},[64-67] to create the most oxidizing agent in biology, a radical cation ($P680^{\bullet+}$) delocalized among a pair of chlorophylls (P_{D1}/P_{D2}). This oxidizes the Mn_4CaO_x cluster of the OEC in successive one-electron abstraction steps via an intermediary redox-active tyrosine (Y_Z), until the OEC becomes able to complete the four-electron oxidation of water to dioxygen. The intermediate "charging" or "storage" states of the OEC are known as S_i states, where the subscript denotes the number of stored oxidizing equivalents (i = 0–4). S_1 is the resting (dark-stable) state with commonly accepted Mn oxidation states of $Mn(III)_2Mn(IV)_2$, while S_4 is an unobserved transient state that evolves dioxygen (Figure 1). Electron and proton transfers take place alternately,[68] maintaining a narrow potential range for the OEC for all $S_i \rightarrow S_{i+1}$ state transitions. On the electron acceptor side of PSII a plastoquinone is doubly reduced and released from the complex to transfer reducing equivalents further along the photosynthetic chain, eventually to be used in CO_2 fixation.

Our primary focus here is on the site of water oxidation and the contributions of quantum chemistry in understanding its nature, its

This journal is © The Royal Society of Chemistry 20xx

Please do not adjust margins

Please do not adjust margins

properties, and its function. We will cover selected developments and applications in recent years, mostly from our group, that had significant impact on discovering specific correlations between structural features and spectroscopic properties of the OEC, and which contributed to interpreting experimental results and directing further investigations. We will also identify outstanding challenges that will require more than simple extensions of present quantum chemical approaches to be successfully met in the future.

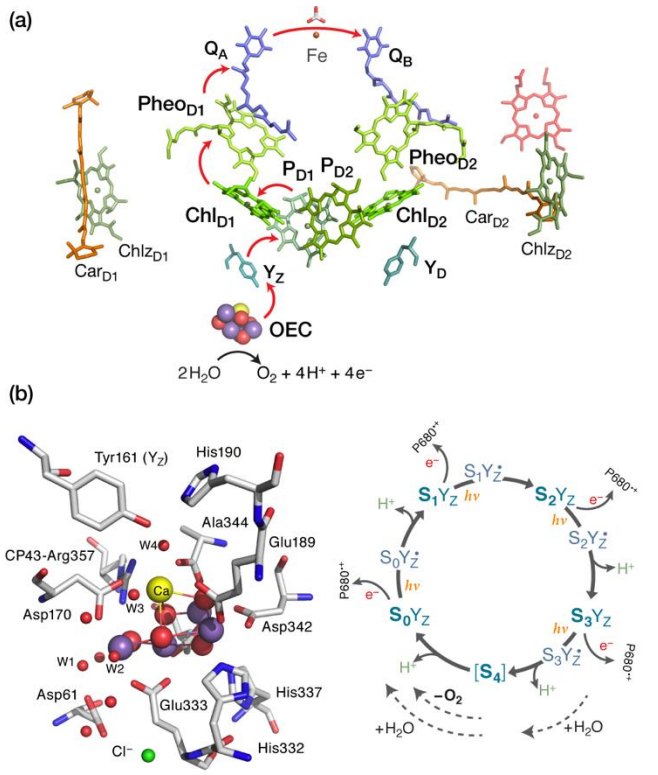

Figure 1. (a) Photosystem II cofactors participating in electron transfer. (b) The oxygen-evolving complex and the catalytic cycle (Kok–Joliot cycle) of the S_i oxidation states including tyrosyl radical intermediates.

2.1. Correlating molecular structure with spin states

For a long time geometric information on the OEC was confined to metal–metal distances derived from EXAFS.[69] This allowed discussion of plausible structural features but could not lead to well-defined atomistic model that are required for quantum chemical investigations. Even the first crystallographic models[70-72] were not of sufficient resolution to allow definition of a unique structure. Therefore, early computational studies[73, 74] explored a range of geometric and mechanistic possibilities but incorporated numerous structural assumptions that later proved inaccurate. Crystallographic models of sufficiently high resolution that appeared in the last decade and that more recently utilize pulses from X-ray free electron lasers changed this situation by accurately defining the spatial arrangement of metal ions and oxygen bridges as well as the type and mode of coordination of first and second sphere ligands.[75-81] As shown in Scheme 1a the core of the OEC consists of four Mn and one Ca ions connected by oxo bridges and additionally bridged mostly by carboxylate residues, while there are also two terminal water-derived ligands (H_2O or OH) on each of Mn4 and Ca. The redox-active tyrosine residue (Tyr161, or Y_Z) is in close proximity and interacts with Ca and the rest of the inorganic cluster via hydrogen bonding. Ambiguities remained,[82] and they still do,[17] for example regarding the protonation states of oxo bridges and the extent of radiation-induced reduction of metal ions,[83-85] but these advances nevertheless enabled quantum chemical studies to be performed on a much safer basis than ever before.[86] One important consequence was that the spatial arrangement was sufficiently well defined to allow theoretical studies of electronic structure, spin states, and spectroscopic properties beyond superficial energy comparisons, thus enabling for the first time direct connections between quantum chemical studies and the vast repository of spectroscopic observations on various catalytic intermediates.

The most obvious target property to begin with is the spin state of specific catalytic intermediates, which in many cases had been identified, or at least constrained, by EPR spectroscopy. Advances in this direction were tied to the investigation of magnetostructural correlations and began with the spectroscopically well-studied S_2 state of the OEC and synthetic analogues. The S_2 state was long known to exhibit two types of EPR signal that correspond either to a low-spin (S = 1/2, $g \approx 2$) multiline state or to a higher-spin state ($S \geq 5/2$, $g \geq 4.1$).[87-92] A landmark study in 2012 established a correspondence between two structural forms of the OEC core and these two spin states.[93] The structural forms were derived from refinement of the 2011 crystallographic model.[75] They were almost isoenergetic and featured different distribution of Mn valences (III-IV-IV-IV versus IV-IV-IV-III) and slightly different connectivity of an oxo bridge that led to their description as open-cubane (S_2^A) and closed-cubane (S_2^B).[93] As will be explained below, quantum chemical investigations of the spin-dependent properties of these models supported their association with the two observed EPR signals.

The quantum chemical approach used for determining the spin states is based on a generalization of the two-centre broken symmetry (BS) DFT methodology[94-97] to the tetranuclear case. The low-lying states of a cluster representing the OEC can be described using the effective Heisenberg–Dirac–van Vleck Hamiltonian (HDvV), which describes magnetic levels in terms of fictitious interactions between local spin magnetic moments:

$$\hat{H} = -2\sum_{i>j} J_{ij}\,\hat{\boldsymbol{S}}_i\hat{\boldsymbol{S}}_j$$

where $\hat{\boldsymbol{S}}_i$ and $\hat{\boldsymbol{S}}_j$ are the spin operators and J_{ij} are the pairwise exchange coupling constants that parameterize the fictitious spin interaction. The sign of J_{ij} signifies whether the interaction is antiferromagnetic ($J_{ij} < 0$) or ferromagnetic ($J_{ij} > 0$). Diagonalization of the Hamiltonian yields the spectrum of spin states ("spin ladder") that can be directly compared to experiment as long as the effective Hamiltonian is a valid representation of low-energy states. The broken symmetry approach attempts to determine the J_{ij} parameters employing a set of Kohn–Sham determinants in which

Please do not adjust margins

Please do not adjust margins

the unpaired electrons are localised at the spin sites (in the present case, the Mn ions) in all possible mutual up/down (α/β) combinations while maintaining the high-spin electronic configuration on each spin site. Using as an example the S_2 state of the OEC mentioned above with Mn oxidation states III-IV-IV-IV, with local S_z of 2 for the d^4 ion Mn(III) and 3/2 for the d^3 ion Mn(IV), then the high-spin determinant can be described as |+2, +3/2, +3/2, +3/2> (or "αααα", M_S = 13/2) and BS determinants are created by flipping local spins of Mn ions. For example, |+2, +3/2, +3/2, -3/2> ("αααβ", M_S = 7/2) or |+2, -3/2, -3/2, +3/2> ("αββα", M_S = 1/2). Each BS determinant is characterized by an M_S value and not S, because it is not a spin eigenfunction. The energies of the BS determinants in combination can be used to extract a set of J_{ij} values for the reduced S_z-only (Ising) Hamiltonian, and subsequently the same set of exchange coupling constants is used to diagonalize the full HDvV Hamiltonian and obtain the spin ladder. The details of the procedure have been described extensively in the literature.[98-100] Figure 2 provides a schematic flow diagram that summarizes the points made above.

This lengthy procedure obviously involves significantly increased computational and human effort compared to studies that simply ignore the spin state problem. For each structural model to be considered one has to perform a series of calculations that often exhibit challenging convergence behaviour, and then perform an array of additional analysis to extract exchange coupling constants and, eventually, the magnetic spin states.

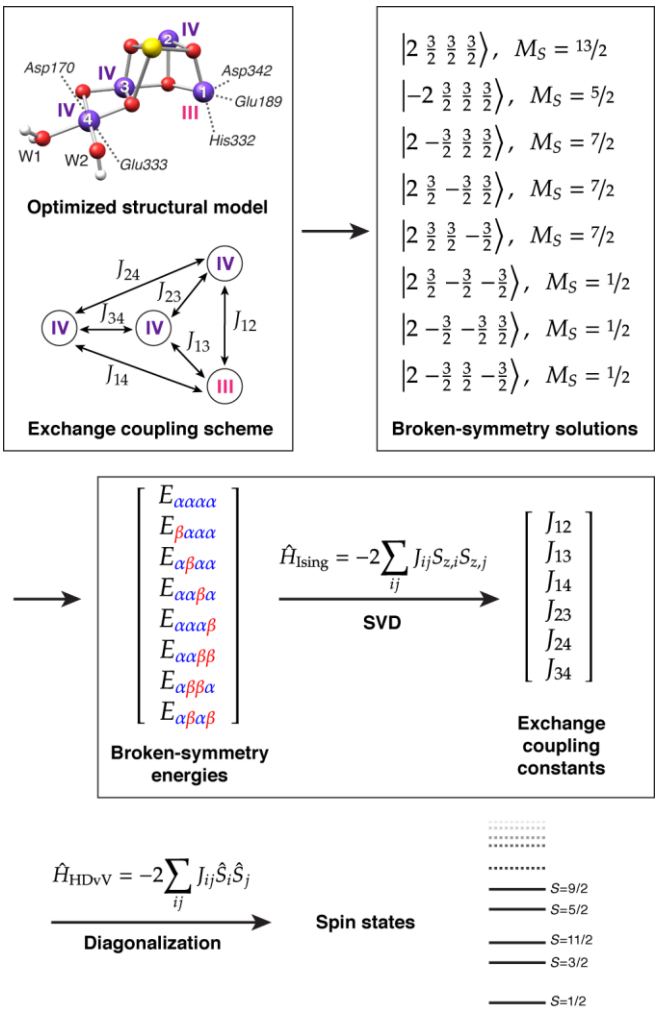

Figure 2. Flow diagram of calculations in the context of the broken-symmetry DFT approach for determining the exchange coupling constants and spin state ladder for a computational model of the S_2 state of the OEC, assuming Mn oxidation states of III-IV-IV-IV. Note that in this case there are only seven BS determinants that can be formed in addition to the high-spin determinant, yet the proper solution to the exchange coupling problem yields in total 320 states (including sublevels of spin multiplets).

Yet, despite the considerable overhead, the results have been richly rewarding and have pushed research in natural water oxidation in new and fruitful directions. It is crucial to stress that no discussion of spin states can be made based solely on any one broken-symmetry solution or by simply comparing energies of different broken-symmetry solutions. Broken-symmetry determinants are not spin eigenfunctions and they do not correspond to observable states. It is an unfortunate fact that several papers erroneously discuss spin states by direct reference to broken-symmetry solutions.

The application of the approach to the two valence isomers found for the S_2 state of the OEC showed that they differed substantially in their exchange coupling scheme (Figure 3).[93] The isomer labelled as S_2^A (III-IV-IV-IV) has antiferromagnetic interaction between Mn1-Mn2 and Mn3-Mn4 resulting in a spin S = 1/2 ground state, whereas S_2^B features strong ferromagnetic interactions within the cuboidal Mn1-Mn2-Mn3 unit (effective spin of the cube S = 9/2) resulting in a total ground state spin of S = 5/2 for this isomer. This

This journal is © The Royal Society of Chemistry 20xx

Please do not adjust margins

Please do not adjust margins

suggests already a potential correspondence between the two structural models and the observed spin states. This was further supported by explicit simulations of EPR spectra, which associated the S_2^A with the *g*=2 EPR signal and the S_2^B model with the *g*=4.1 signal.[93]

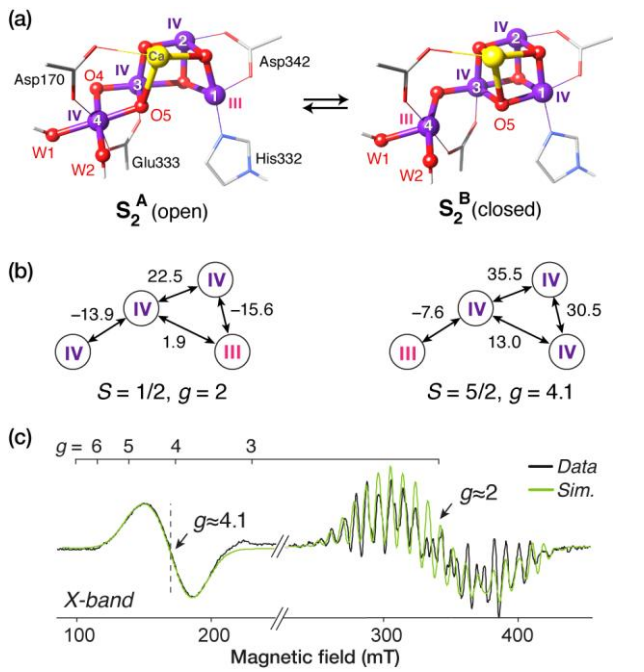

Figure 3. (a) Computational valence isomer models for the S_2 state of the OEC. (b) Computed nearest-neighbor exchange coupling constants and resulting spin states. (c) The valence isomers rationalize the two EPR signals associated with the S_2 state. In addition, they are very close in energy and interconvertible over a low barrier, as required experimentally, and they are each consistent with independent spectroscopic measurements for each *g* signal, including the ^{55}Mn hyperfine coupling constants and the distinct localization of the Mn(III) ion in each case.

Importantly, the results on the magnetic properties of the S_2 state isomers are aligned with experimental and theoretical results on synthetic trinuclear and tetranuclear analogues.[101, 102] For example, synthetic $Mn(IV)_3Ca$ cubane complexes[22, 103] that mimic this structural unit of the S_2^B model similarly have dominant ferromagnetic coupling among their Mn ions and display high-spin (*S* = 9/2) ground states.[102] This can be explained at the orbital level by elimination of superexchange interactions between the Mn ions due to the angles of the oxo bridges.[102] The broken-symmetry approach can be equally well applied to spin-frustrated systems with antiferromagnetic ground states, as exemplified by a combined experimental and theoretical study of a low-spin trinuclear terpyridine cluster with a $Mn(IV)_3O_4$ core.[101]

Consideration of spin state alone may be insufficient to establish a firm one-to-one correspondence between a computational model and a true catalytic intermediate. For example, other structural models or protonation patterns can be shown to have the same spin state as that observed experimentally,[104, 105] but it is only via the combined evaluation of geometries, spin states, energetics, and spectroscopic parameters that safe assignments can be reached. In any case, spin states are strong constrains and essential for discussing the relevance of any computational model to an experimentally observable state of the physical system. Thus, they have been part of many further studies that examined the nature of specific intermediates, by showing connections between structural features and magnetic properties. For example, BS-DFT analysis of spin states for various possible isomeric forms of the S_3 state established that the *S* = 3 states observed by magnetic resonance spectroscopies[106-108] must be attributed to structural forms that have one additional water-derived ligand compared to the preceding S_2 state, and hence forms where all four Mn ions are six-coordinated.[104, 106] By contrast, a form of the S_3 state that has no additional ligand and contains a five-coordinated Mn(IV) ion is characterized by the highest possible spin for a $Mn(IV)_4$ cluster, of *S* = 6 (Figure 4).[108, 109]

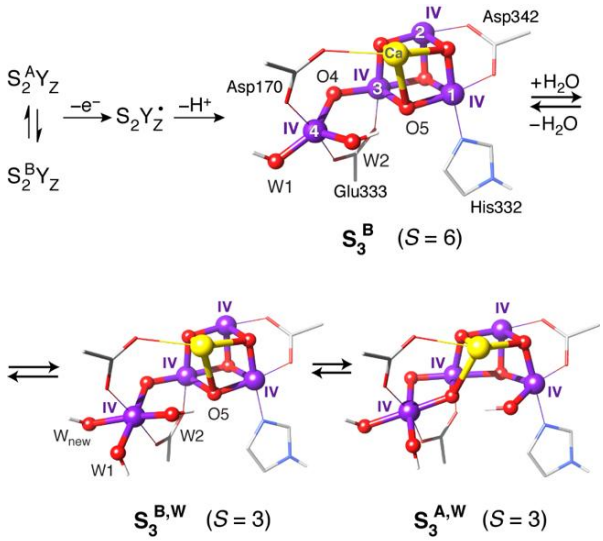

Figure 4. Possible structural components of the S_3 state of the OEC with their corresponding spin states.

Similar structure–magnetism correlations have been used to examine the effect of protonation of oxo bridges on specific exchange coupling pathways. It is known that in general an oxo bridge enables stronger superexchange and thus enhances antiferromagnetic coupling between two Mn ions compared to a hydroxo bridge.[110-112] Applied to the OEC, study of the effects of protonation or hydrogen bonding to specific oxygen bridges contributed, among others, to screening of structural models for the S_0 state[104, 113] and to evaluation of possibilities for the interaction of small molecules such as methanol and ammonia with the manganese cluster.[114-117] It is also important to note that since different oxidation states of the Mn ions lead to different exchange interactions, analysis of magnetic properties in terms of exchange couplings and spin ladders is essential for evaluating redox-isomeric forms of specific S-state intermediates[104] and for evaluating competing oxidation state paradigms.[104, 118, 119]

These successful applications should not obscure the fact that the spin-projected broken-symmetry DFT methodology, even if applied correctly, depends considerably on the nature of the functional, on the nature of the system under study, and on the validity of the effective spin Hamiltonian assumed to describe the

Please do not adjust margins

Please do not adjust margins

system. High-valent/high-spin manganese systems are among the most favourable systems for this approach. Indeed, according to a study by Krewald et al.,[104] the broken-symmetry approach using the TPSSh functional and the complete methodology for calculation of exchange coupling constants and spin states predicts with absolute accuracy the correct ground spin state of all known oligonuclear manganese complexes with oxidation states relevant to the OEC. Exceptions may be associated with limitations of the isotropic exchange model rather than with failures at the DFT level. Of course, even if the energetics obtained by the above procedure are useful, it is always desirable to have direct access to the spin states themselves, which can only be achieved by using multireference methods. For multi-electron systems such as those containing high-valent Mn ions, multireference approaches have found limited application so far.[120, 121] Notable studies that are directly relevant for the OEC include the use of density matrix renormalization group (DMRG) based complete active space self-consistent field (CASSCF) and *N*-electron valence state perturbation theory (NEVPT2) calculations on dinuclear Mn and Cr complexes.[112, 122, 123] Such calculations are far from trivial. They require careful study of convergence with respect to the active space and other technical parameters, and they present a series of requirements that must be satisfied for the results to be meaningful and reliable. As defined by Roemelt et al.,[122] these requirements include the necessity for state-averaged orbital optimization over all spin multiplets that are part of the exchange coupling problem and the necessity to include dynamic correlation. Results obtained without state averaging, without complete orbital optimization, and without additional treatment of dynamic correlation are numerically inadequate and may show substantial deviations from the correct order and spacing of spin states. In cases where such deviations have been reported for non-manganese systems,[124, 125] it is not always clear whether the correct application of the methodology as defined above would suppress or eliminate them.[126] Systems with more than two Mn ions present profoundly greater difficulties for such methods. This is not strictly because of the larger active space but because of how the calculations should be performed in order to enable us to derive and discuss magnetic properties. Although state-specific DMRG-based CASSCF calculations have been demonstrated for tetramanganese models,[127, 128] these calculations have not dealt with, and cannot address, the questions of exchange coupling and spin state energetics; it cannot even be verified in principle that the correct ground state is computed. The above stated requirements derived from application of DMRG-CASSCF/NEVPT2 on a dinuclear Mn complex,[122] particularly the need for state-averaged orbital optimization over all magnetic spin levels, imply a steep increase of computational complexity and cost for exchange coupling analysis of a trimanganese system, which is an open challenge for multireference treatments, and probably render the tetranuclear case intractable with standard algorithms on conventional computers.

2.2. Spectroscopic parameters

In addition to spin states, an important point of contact between quantum chemistry and experiment are the various forms of spectroscopy used to study catalytic intermediates of the OEC. Here we focus only on parameters relevant to magnetic resonance spectroscopies. Spectroscopy-oriented quantum chemistry is more than a powerful tool for analysing experimental results and more than a way of maximizing the extraction of information from experimental spectroscopic data. It allows access to information that lies beyond the limitations of specific experimental approaches and can achieve unification of disparate sources of information into a common interpretation that connects experimental observations with the electronic structure of computational structural models.

Hyperfine coupling constants of Mn ions contain rich information on the local and global electronic structure of the OEC. Here the great challenge for quantum chemistry has been how to properly compute Mn HFCs for an oligonuclear exchange coupled system with DFT. This was addressed with the development of a generally applicable theoretical methodology that allows the use of the standard broken-symmetry DFT approach and makes connections between the various levels of Hamiltonian approximations involved in the fitting of HFC parameters from experimental spectra and in the calculation of HFCs from approximate DFT.[98] The interested reader is referred to the original publication for methodological details.[98] It is noted that for comparisons to experimental values a scaling factor has to be used for the final spin projected HFCs because of the systematic underestimation of core spin polarization by DFT.[129, 130] This factor is not universal and may differ depending on details of the methodology such as the type of functional and the treatment of relativity, as well as on the reference set of compounds used to derive the required scaling.[98, 99, 110, 131-133] New theoretical developments in this area will be important for making the calculations of HFCs by DFT more robust.[134, 135] Recent advances in the calculation of HFCs by correlated wave function methods such as coupled cluster theory[136] are also very promising but their applicability and reliability remain incompletely explored.[137]

Following a pilot application[98] on a synthetic tetramanganese complex that is a Mn(III)Mn(IV)$_3$ analogue[138] of the S_2 state, broken-symmetry DFT was used in combination with the above method to compute spin states and hyperfine coupling constants of a wide variety of structural models that were considered at the time as geometric possibilities for the OEC.[99] This study showed that many ideas derived from EXAFS studies[139] as well as practically all models reported in computational studies until that time[140-143] were not consistent with the spectroscopic data on the S_2 state. These methods were essential in establishing that model S_2^A described in Figure 3 corresponds very well with the ^{55}Mn HFCs determined experimentally by ENDOR spectroscopy,[144-150] with one large, two medium, and one smaller hyperfine coupling constant.[93] These results demonstrated the importance of spectroscopy-oriented quantum chemistry in discriminating between structural possibilities and encouraged numerous subsequent applications to the OEC and other exchange-coupled oligonuclear systems, including refinements and extensions of the method.[131, 151-154]

An obvious use of quantum chemistry in the study of ^{55}Mn HFCs is in the evaluation of different oxidation state possibilities, both in

This journal is © The Royal Society of Chemistry 20xx

Please do not adjust margins

Please do not adjust margins

terms of absolute oxidation levels for the whole cluster and in terms of internal distribution of local oxidation states (valence isomeric forms) for a given total oxidation level or S-state intermediate. This approach has been adopted for evaluating various isomers of the half-integer-spin S_0 and S_2 states that have been studied extensively by ENDOR spectroscopy.[144-148] In particular for the S_0 state the situation arises where in principle the total number of unpaired electrons can be distributed among the four Mn ions with a formal $Mn(III)_3Mn(IV)$ or $Mn(II)Mn(III)Mn(IV)_2$ configuration. In combination with analysis of exchange coupling and spin states, computed ^{55}Mn HFCs have helped in evaluating various possible structure models.[104, 113] Another important use of computed ^{55}Mn HFCs has been in the evaluation of possible models for the S_3 state. ENDOR-detected NMR studies on one of the components of this state showed that all Mn ions were electronic similar and isotropic.[106] Quantum chemical calculations helped to show that all-Mn(IV) cluster models where all Mn ions are octahedrally coordinated due to coordination of an additional water-derived ligand compared to the S_2 state are most consistent with the data.[104, 106] This carries significant weight for the persistent question of whether the $S_2 \rightarrow S_3$ transition involves metal-centred or ligand-centred oxidation.[155-157] The calculations firmly support the Mn-centred option because they demonstrate that the experimentally determined ^{55}Mn HFCs for the S_3 state are not reproduced with a $Mn(III)Mn(IV)_3$ cluster such as in the preceding S_2 state. Owing in part to its heterogeneous nature, as clearly revealed by various magnetic resonance spectroscopic studies[106-108, 158-160] – though not resolved by currently available structural methods which can only provide spatially or temporally averaged representations– the composition of the S_3 state remains under investigation.[161-164]

^{55}Mn HFCs have also been used in evaluating possible protonation states of oxo bridges and Mn-bound water-derived terminal ligands, and hence determine the most likely overall protonation level and pattern of the active site.[100, 104] This analysis eliminated the possibility of bridge protonation in the S_2 state and led to the conclusion that the terminal Mn4 ion in the S_2 state is most likely ligated by one water and one hydroxo ligand (W1 and W2 in Figure 1).[100] The focus on spectroscopic properties enables direct screening of computational models against experimental constrains and therefore guides the study of the catalytic mechanism in ways that are otherwise impossible.

Although emphasis in the above was placed on metal ions, ligand HFCs provide significant additional information. It is possible to use ligand HFCs (e.g. of Mn-coordinating oxygen or nitrogen nuclei) to assign metal oxidation states,[165] to study the identity and kinetics of exchangeable atoms, and to discover the mechanisms by which small molecules access the active site and interact with the Mn ions.[114, 115, 166-171] An example that will be highlighted here concerns the interaction of the substrate analogue methanol with the OEC cluster. The importance of these studies is that they point to likely pathways for substrate delivery to the OEC. It has long been known that methanol modifies the magnetic energy levels and EPR signals of the manganese cluster of the OEC, but the access pathway(s) and mode of interaction remained unknown.[167, 172-178] Based on the experimental determination of the ^{13}C hyperfine parameters of isotopically labelled methanol interacting with the S_2 state of the OEC,[167] an extensive computational screening of structural models was carried out that involved calculation of spin state energetics and ^{13}C isotropic and dipolar HFCs for each one.[116] This led to rejection of several possibilities such as direct binding of methanol to Ca^{2+} or one of the Mn ions, supporting instead a second-sphere interaction that resulted in reorganization of the hydrogen bonding network affecting the O4 bridge and the Mn3–Mn4 exchange coupling interaction.[116] This is in contrast to the case of ammonia, which binds directly to Mn4,[115, 170, 171, 179] at least in one of its interaction modes. The identification of a crucial difference between cyanobacteria and higher plants in a residue close to the proposed site of methanol binding (D1-N87A)[117] is consistent with the different response of plant versus cyanobacterial OEC to methanol, which can be explained by the restricted accessibility in the case of cyanobacterial OEC due to the more constrained channel architecture.[117]

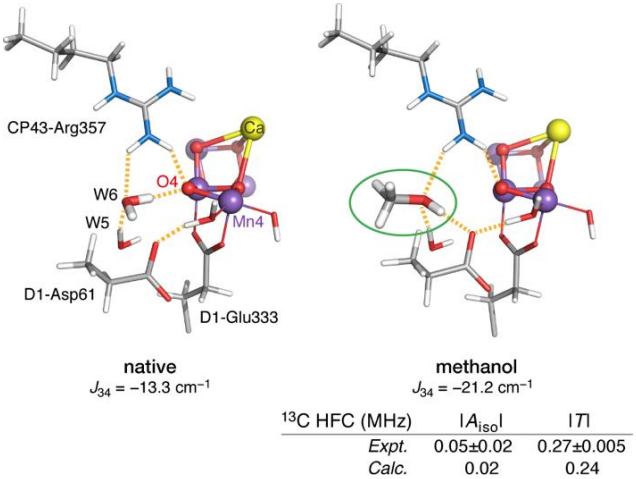

Figure 5. Proposed model for interaction of methanol with the OEC.[116] The increase in Mn3–Mn4 antiferromagnetic exchange coupling explains the stabilization of the low-spin S = 1/2 state of the cluster. The model is the only one of those examined that simultaneously agrees with the experimental ^{13}C hyperfine coupling parameters of Oyala et al.[167] Figure adapted from Ref. 116 – Published by The Royal Society of Chemistry.

An important methodological advance in terms of studying and understanding the local anisotropy of the Mn ions was been the development of the local complete active space configuration interaction (L-CASCI) approach.[180] This enables the use of multireference methods for the calculation of local zero field splitting tensors and consists in conducting a multireference (CASCI) calculation with an active space specifically constructed to contain local orbitals for any given metal ion. Successive application of the method for each centre of interest eventually yields all on-site parameters for further analysis. Application of the L-CASCI approach to the S_2 state models of Figure 3 allowed the explicit calculation of site ZFS tensors (specifically the spin-orbit coupling contribution D_{SOC}) for the Mn(III) ions in each valence isomer (Figure 6).[180] The orientation of the D_{SOC} principal axes correlate directly with the orientation of the pseudo-Jahn–Teller axes of the Mn(III)

Please do not adjust margins

Please do not adjust margins

ions, which are oriented along the formally open coordination site of Mn(III) in each isomer. Importantly, the valence distribution, geometric parameters, and computed local ZFS for the Mn4(III) ion in the valence isomer S_2^B agree perfectly with analogous experimental studies of the g≈4.1 component of the OEC,[181] With D_z oriented along the W2-Mn4-O5 axis. This strongly supports the assignment of S_2^B to the high-spin g≈4.1 signal, in contrast to other hypotheses that do not place the Mn(III) ion at the Mn4 site. The L-CASCI approach will certainly see increased use in the future as more in-depth analysis of catalytic intermediates is undertaken, not only for other intermediates of the OEC but also for other biological or synthetic clusters with multiple open-shell transition metal ions.

Quantum chemical studies that focus on spectroscopic properties have also helped to elucidate critical aspects of the redox-active tyrosine Y_Z and Y_D residues.[182, 183] Here it is the g-tensor of the tyrosyl radical that is the central spectroscopic parameter. This can be calculated with standard DFT approaches, although particular care has to be taken to ensure that the calculations correctly represent the electronic structure of both the Y_Z radical and the Mn cluster. Most relevant for the OEC are studies that focus on the nature of tyrosyl radical intermediates formed during the $S_2 \rightarrow S_2Y_Z^{\bullet} \rightarrow S_3$ transition.[109, 182] Detailed investigations of the initial stages of the $S_2 \rightarrow S_3$ transition showed that formation of the tyrosyl radical is accompanied by reorientation of the dipole moment of the OEC in the S_2^B state,[182] which likely triggers proton release from the terminal water ligand W1 of the Mn4 ion to the second-sphere Asp61 residue that acts as proton acceptor.[184-186]

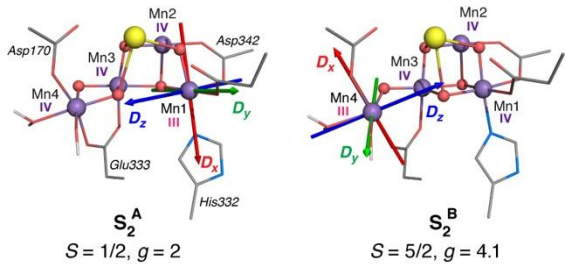

Figure 6. Orientation of principal axes of the D_{SOC} for the five-coordinate Mn(III) ion in each isomer of the S_2 state of the OEC, computed with the L-CASCI approach. Adapted with permission from Retegan et al.[180] Copyright 2014 American Chemical Society.

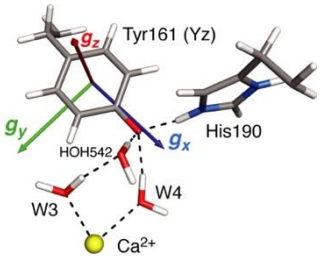

Figure 7. Orientation and components of the g-matrix for the $S_2^BY_Z^{\bullet}$ state according to Retegan et al.[182] with DFT-computed values g_x = 2.0054 > g_y = 2.0042 > g_z = 2.0022. The immediate hydrogen bonding environment of the radical is also depicted.

This deprotonation is necessary for subsequent oxidation of the Mn ion by the tyrosyl radical.[109] Y_Z oxidation is accompanied by shifting of the phenolic proton to His190. The ultimate fate of this proton is still under investigation.[187-189] In terms of the spectroscopic properties of the formed tyrosyl radical, Retegan et al.[182] established a clear correlation between the hydrogen bonding environment and the g values of the tyrosyl radical. The g_x component is oriented along the C–O bond and its correlates almost linearly with the change in the spin population of the phenolic oxygen, the atom with the largest spin-orbit coupling contribution. The spin population is in turn correlated with the number of hydrogen bonds and the electron affinity of the tyrosyl radical. This makes the g_x value a direct probe of the hydrogen bonding environment and of the redox potential of $Y_Z^{\bullet}$. In the native system the g_x value was relatively low compared to analogous literature precedents, which was attributed to the presence of three hydrogen-bonding interactions, two from adjacent water molecules and one from the His190 proton (Figure 7).[182]

Similar correlations derived from quantum chemical studies have been essential for probing the hydration and uncovering the structural basis of spectroscopic observations for the other redox-active tyrosine of PSII, Y_D.[183] Intriguingly, the above observations suggest a direct role for Ca in structuring the hydrogen-bonding environment of Y_Z and hence directly modulating its redox properties,[182] which is crucial for ensuring efficient coupling between the manganese cluster of the OEC and the charge-separation site (reaction centre) of PSII. Complementing this hypothesis, explicit calculations of the effect of calcium substitution by various redox-inactive cations showed that the redox potential of the OEC responds only to the total charge of the cation while remaining insensitive to its Lewis acidity,[190] in contrast to correlations established for synthetic complexes.[190-192]

2.3. Challenges in computational setup and modelling

The preceding sections highlighted contributions of quantum chemistry to understanding Nature's water oxidizing catalyst from the perspective of predicting magnetic and spectroscopic properties. However, it should be stressed that the use of an appropriate theoretical method or procedure to calculate geometries, energies, or other properties, in no way ensures attainment of reliable results that can be meaningfully correlated with experiment and used to evaluate computational models. This is because there are often practical aspects relating to the definition and treatment of the atomistic model itself that may introduce weaknesses which undermine the overall reliability of quantum chemical studies regardless of the "intrinsic" ability of any given theoretical method to deliver high quality numbers. Unfortunately such weaknesses may remain unnoticed because the results obtained by calculations on inappropriate models are rarely, if ever, noticeably wrong in an absolute numerical sense. Here we single out a few issues in model setup that may compromise the relevance of computational results for understanding the real system. Although the examples are taken from OEC studies, the broader lessons are universally valid.

When dealing with large and complex active sites such as the OEC, a principal concern is to build a quantum mechanics (QM) cluster model large enough to incorporate the effects of the

 This journal is © The Royal Society of Chemistry 20xx

Please do not adjust margins

Please do not adjust margins

immediate environment directly or indirectly. The QM model needs to be large enough to explicitly include the complete first coordination sphere and all elements of the second coordination sphere that interact via hydrogen bonding. Information about the structure of the protein matrix that is not explicitly included in the QM cluster model is included indirectly by constraining specific atoms. Constraints are typically applied to backbone atoms such as α-carbons and groups used to terminate peptide chains. When the QM cluster model omits hydrogens bonds that are present in the crystal structure, then additional geometric constraints may be considered, e.g. of specific dihedral angles, or at least optimized models should be examined very carefully for structural compliance with the absent protein matrix. A specific example of this is offered by His332, ligand to Mn1. Inspection of the complete environment of the OEC shows that the orientation of the His332 imidazole ring is restrained by a hydrogen bonding interaction with the peptide carbonyl of Glu329 (Figure 8), which normally would not be included in QM cluster models of the OEC. The absence of this interaction may result in rotation of the His332 ring by ca. 90° during geometry optimization. Retegan et al. showed that such rotation directly affects the ^{55}Mn hyperfine parameters for Mn1 by modifying the nature of the Mn–N bonding.[193] Moreover, the incorrect rotation of His332 artificially increases the accessibility to Mn1, for example by water molecules. Therefore, the orientation of this residue affects considerably the computed relative energetics for water or hydroxy binding and the relevant models reported in the computational literature should always be scrutinized for structural correctness.

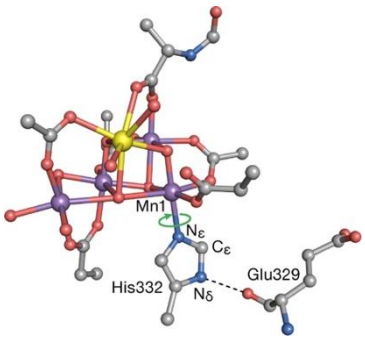

Figure 8. The His332–Glu329 hydrogen bonding interaction constrains the imidazole plane of the histidine residue. Computational models that do not take this into account lead to incorrect description of the coordination sphere of Mn1 and all processes and properties associated with it. Adapted with permission from Ref. 193. Copyright 2013 American Chemical Society.

The combination of quantum mechanics with a force-field (molecular mechanics) treatment of the environment, i.e. the QM/MM approach, has a strong tradition in the OEC[140, 186, 193-195] and it is expected to offer a better treatment of the environment when applied correctly. Here we would stress that the use of the QM/MM approach rarely allows for appreciable reduction in the size of the QM region compared to a standard QM cluster approach and does not negate the need to incorporate all important hydrogen bonding groups (including essential crystallographic waters) in the QM region. In fact, the use of a very small QM region leads with certainty to artefacts, which include spurious redox activity arising at the periphery of the QM region that results from redox imbalance (see below) or overpolarization from force-field charges.

Related to the above is the inclusion of the redox-active Tyr161 residue (Y_Z) in QM cluster models, or in the QM region of QM/MM models. Y_Z is both structurally coupled to the rest of the OEC via a tight network of hydrogen bonds, and redox-coupled as amply evident by the catalytic cycle depicted in Figure 1 and by preceding discussions. Thus, omission of the Tyr161–His190 pair from computational models can lead to two critical artefacts: a) removal of the hydrogen bonding network and drastic reorganization of the water molecules that are situated between Y_Z and the Mn ions, and b) absence of redox balance in the computational model, or inability to evaluate it. The first issue means that in the absence of the Tyr161–His190 pair and of the physiological associated hydrogen bonding network, calculations of hypothetical processes implicating these waters have unnaturally low barriers and little physical connection to the real system. The second issue means that without the tyrosine and without explicitly studying the relative energies of $S_iY_Z^{\bullet}$ versus $S_{i+1}Y_Z$ states, no credible discussion of S-state transition energetics can be made. Explicit consideration of Y_Z and of its redox role is not only essential when S-state transitions are examined or when Y_Z participates directly in the mechanism.[109, 182, 196-198] The redox properties of any computational model should be examined as standard practice to ensure that intrinsic redox balance is achieved and that no unphysical properties are inadvertently introduced. For example, a recent study showed that a set of assumptions regarding Mn oxidation states and protonation states of specific ligands results in the unphysical shifting of the site of subsequent oxidation from Y_Z to the second-sphere histidine His337.[199]

2.4. Catalytic progression and O-O bond formation

The precise details of the water oxidation mechanism during the later stages of the catalytic cycle remain a constantly evolving discussion.[17, 200-202] Open questions revolve around the steps of the $S_2 \rightarrow S_3$ transition, the composition of the heterogeneous S_3 state and the "active" population of S_3 state that progresses further to form the O–O bond. Very little, and often indirect, experimental data exist on the $S_3Y_Z^{\bullet}$ intermediate and the most critical part of the cycle that involves dioxygen evolution and reconstitution of the S_0 state.[203-205]

The two valence isomeric forms of the S_2 state of the OEC depicted in Figure 3 were shown to behave differently upon oxidation. Independent computational studies confirmed that after formation of the tyrosyl radical intermediate, the valence isomer with the Mn(III) ion at the Mn4 site, $S_2{}^{B}Y_Z^{\bullet}$, is the one where the tyrosyl radical can be reduced by manganese so that the cluster advances to a $Mn(IV)_4$ S_3 state[109, 197] (see above for comments regarding the irrelevance of computational models that do not explicitly incorporate the Y_Z–His190 pair and hence neglect the central question of redox balance between the manganese cluster and the redox-active tyrosine). Although various other possibilities may be envisioned, at this time the above $S_2 \rightarrow S_3$ sequence appears to be the best attempt so far to accommodate most experimental

Please do not adjust margins

Please do not adjust margins

observations on S_2, $S_2Y_Z^{\bullet}$ and S_3 states, particularly from EPR spectroscopy.

In the above scenario a key species is the S_3 component with a five-coordinate Mn(IV) ion (S_3^B in Figure 4), which must have a high spin state (S = 6) as predicted by the quantum chemical analysis of Retegan et al.[109] This has received very strong experimental support by a recent multifrequency EPR experimental study of the S_3 state in spinach PSII, which directly identified an S=6 population with high effective anisotropy deriving from anisotropic exchange coupling between the coordinatively unsaturated Mn4(IV) ion and the $Mn(IV)_3Ca$ cubane subunit.[108] Importantly, the S=6 component was found to be the exclusive species in methanol-treated spinach PSII and to form a major part of S_3 even in the native system.[108] Although the water bound intermediate-spin (S=3) isomers of Figure 4 have been experimentally confirmed as distinct populations of the S_3 state, Krewald et al. showed that water binding is not required to oxidize the cluster to the S_4 state.[206] Assuming the water-unbound form is catalytically active, this would allow Mn-based oxidation, leading to an S_4 state of the OEC with a five-coordinate Mn4(V) ion bearing a terminal oxo group at the formally "W2" position of earlier states.[206] This can then couple nucleophilically in an acid–base with the internal oxo bridge to form the O–O bond (Figure 9a).[206] The above mechanism is the only currently discussed possibility that allows for complete separation of the charging phase (four Mn-cantered oxidations) from the actual catalytic phase, which can be achieved by even-electron O–O bond formation even in a single concerted step.[206]

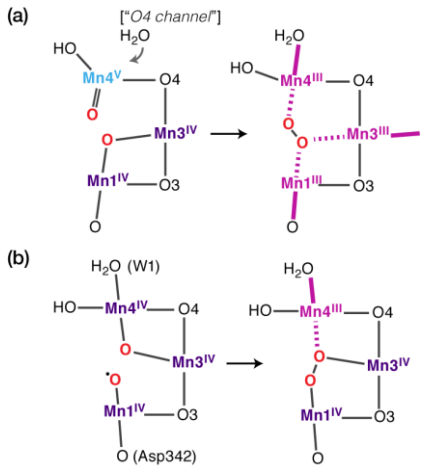

Figure 9. Schematic depiction of two possibilities for the O-O bond formation step in the S_4 state. (a) Creation of a Mn(V)=oxo species from a preceding water-unbound conformation of the S_3 state enables even-electron intramolecular nucleophilic coupling that resets the cluster to the S_0 oxidation state level. (b) Creation of a Mn(IV)-oxyl intermediate leads to radical oxyl–oxo coupling.

On the other hand, if a water-bound S_3 species is the active population of S_3, then it is expected that the more stable $S_3^{A,W}$ isomer will be involved. The reactivity in this case has been investigated by extensive computational studies and it is expected that the final $S_3 \rightarrow S_4$ step involves ligand-cantered oxidation to create an oxyl radical.[143, 207] This would subsequently couple in a radical oxyl–oxo coupling mechanism (Figure 9b), which can itself be realized in multiple alternatives.[185, 208, 209]

Note that both of the above scenarios involve homovalent $Mn(IV)_4$ S_3 isomers and assume a regular sequence of Mn-centered oxidations at least up to the S_3 state (for a radical oxyl-oxo coupling mechanism) or all the way to an S_4 state (for a nucleophilic oxo coupling mechanism). Several similar or distinct possibilities are being discussed,[81, 161, 162, 164, 210-213] including alternatives avoiding alternative valence isomeric forms for the S_2 state, invoking early water binding before advancement to the S_3 state, assuming formation of an oxyl radical in the S_3 state or even "early onset" O–O bond formation already in the S_3 state, and others. Some of these alternatives may be in explicit or implicit disagreement with the most obvious interpretations of experimental data up to the S_3 state,[161] but in view of the absence of meaningful constraints past the S_3 state, they need to be carefully evaluated and for this reason further and more ambitious experimental and theoretical studies will be required.

A specific challenge for quantum chemistry in this case is to accurately distinguish energetically between different redox isomeric forms. Isobe et al. have already shown the sensitivity and precariousness of DFT when dealing with this problem.[163, 211] The question of accurate energetics in this context is closely related to the general problem of spin-state energetics for transition metal systems,[214] though magnified in complexity by the presence of the four interacting open-shell Mn ions and the potential for oxygen-based radicals and O–O bonded intermediates. Achieving systematically accurate energetics in this case might be possible by a new generation of linear scaling coupled cluster approaches. A prominent example is the domain-based local pair natural orbital approach to the popular coupled cluster theory with single, double, and perturbative triple excitations, i.e. DLPNO-CCSD(T).[215-217] The method has already been applied with success in smaller transition metal systems,[218-221] but the OEC presents much greater challenges. Pilot applications on minimal structural models have been reported but it remains to be seen whether successful applications are possible on realistic models of the OEC.

In the context of electronic structure challenges it should also be noted that the remarks made above regarding the nature of broken symmetry solutions also hold for any other aspect of the system, including DFT-derived mechanistic schemes. The use of a single spin configuration to follow a reaction pathway, particularly a reaction that involves multiple spin states of an exchange-coupled system, is an approximation whose crudeness is impossible to determine beforehand. Without negating the value of straightforward DFT studies in guiding our thinking on the mechanism of water oxidation, it is highly desirable to eventually approach the question of O–O bond formation in the OEC with proper consideration and formally correct treatment of the multireference nature of the process.

3. Hydrogenases

3.1. Background

This journal is © The Royal Society of Chemistry 20xx

Please do not adjust margins

Please do not adjust margins

Evolution led some organisms to develop enzymes with the ability to catalyse the reversible heterolytic splitting/formation of H_2. In contrast to the OEC of PSII, which is unique and identical in all oxygenic photosynthetic organisms, hydrogenases show a wider variability. They are typically divided into three families depending on the transition metal composition of their active site: [Fe], [FeFe] and [NiFe] types.[29] Hydrogenases produce H_2 with turnover frequencies reaching 3.10^4 s^{-1} at 30°C) at marginal potential beyond equilibrium (-400 mV vs NHE, pH = 7).[222] This catalytic activity can only be matched by platinum.[223] Their catalytic efficiency, thermostability, and low overpotentials, make hydrogenases ideal models for the bioinspired synthesis of new organometallic catalysts. However, their complex protein structure and the nature of the reaction they perform have posed obstacles in obtaining a clear and precise view on the details of how they function. The size and composition of the active sites make hydrogenases challenging systems to study also from the theoretical point of view.[224]

The structural elucidation of the [NiFe] hydrogenase revealed an organometallic Ni-Fe complex with CO and CN- ligands bound to Fe,[225] while four cysteine residues ligate the Ni site. Two of the cysteines bridge the two metal ions as shown in Scheme 1b. The nickel center has been suggested to play a critical role in hydrogen binding/proton activation and in the redox chemistry of the catalytic cycle. It is postulated that three different active states are involved during catalysis: Ni-SI_a, Ni-R, and Ni-C.[34] Although broad agreement exists on the presence of Ni–C and Ni-R, uncertainties remain about the completion of the cycle and about how each state converts to the other.

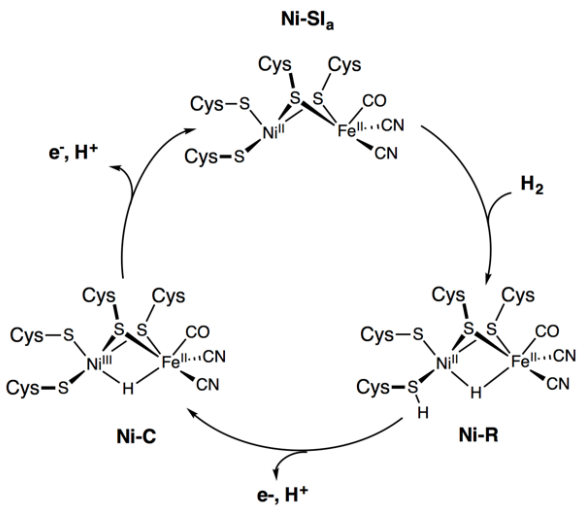

Figure 10. Proposed catalytic cycle of the [NiFe] hydrogenase involving the Ni-SIa, Ni-R, and Ni-C states.

Consequently, there is still lack of consensus on the catalytic cycle of [NiFe]-hydrogenases even if distinct mechanisms have been proposed on the basis of combined experimental and theoretical evidence (Figure 10). In the proposed cycle, H_2 is activated through binding to the diamagnetic Ni-SI_a state, where the metals are present as Ni^{II} and Fe^{II} and have a low spin state. This activation leads to heterolytic cleavage of the H–H bond and the formation of the Ni-R state, which contains a bridging hydrido ligand. The two-electron oxidation of Ni-R regenerates the Ni-SI_a while the second proton is released. The intermediate Ni-C species corresponds to the one-electron oxidized form of Ni-R and is assigned to a $Ni^{III}Fe^{II}$-hydrido complex, which has been experimentally characterized.[226]

The [FeFe] hydrogenase shares some features with the [NiFe] type. Its catalytic center, the so-called H-cluster, is a di-iron center [2Fe] composed of a proximal Fe covalently attached via a cysteine thiol bridge to a cubane-like [4Fe4S] cluster, and a distal Fe, which has an open coordination site for H_2 binding (Scheme 1). Similarly to the [NiFe]-hydrogenase, each iron site binds two CO and CN ligands, with one CO shared between the two metal ions.[227] The ligand sphere leads to Fe^{II} metal centers in the low-spin state. A key structural difference to the [NiFe]-hydrogenase is the presence of a dithiomethylamine (dtma) ligand that bridges the Fe ions.[228]

The catalytic cycle of [FeFe] HG (Figure 11) remains controversial despite extensive research efforts. According to recent reports, binding of H_2 to the oxidized active ready state, H_{ox}, results in the heterolytic cleavage of H_2, and in the formation of H_{hyd}. The latter species is a mixed-valence $Fe^{II}Fe^{I}$ intermediate featuring a protonated dtma and a terminal hydride ligand. On deprotonation, H_{hyd} is converted into the rather stable H_{sred} state with both metals being at the (+I) oxidation state. The one electron oxidation of H_{sred} yields H_{red} before a proton-coupled electron transfer recycle H_{ox}. Overall, the mechanism of the [FeFe] HG remains debated particularly with respect to the one- and two-electron reduced intermediates.[33]

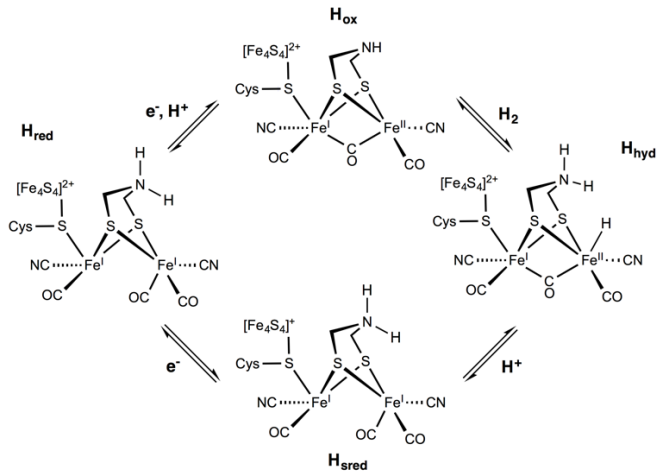

Figure 11. Postulated reaction mechanism of the [FeFe] hydrogenase involving the H_{ox}, H_{hyd}, H_{red}, and H_{sred} states.

The absence of consensus regarding the complete catalytic cycle of hydrogenases has driven developments towards proficient catalysts for HER. Studying smaller catalysts is insightful for the proper design of new molecular electrocatalysts even if they lack the functionally important protein matrix. Many biomimetic and bio-inspired complexes have been developed and investigated with the purpose to understand and mimic the proficiency of

Please do not adjust margins

Please do not adjust margins

hydrogenases. In this respect, computational approaches combined with experiment can play a key role in the development of efficient synthetic catalysts.[229-231] Contributions of quantum chemistry are not limited to rationalizing experimental observations; the correlation between theory and experiment drives conceptual and methodological developments toward new experimentally accessible systems. As in the case of the OEC, studies combining experiment and theory contribute to understanding the properties and reactivity of the enzymes, but they have also assisted more directly in the design of more effective HER catalysts.

In the following, we report on the extensive use of the theoretical methods to better apprehend and get insight into the geometric structures, electronic structures, and properties of hydrogenases as well as related biomimetic and bio-inspired models. We will show that quantum chemical studies are crucial to identify the electronic and thermodynamic parameters that govern the reactivity of catalytic centers, to determine the crucial structural determinants of catalytic activity, and to unravel the key steps of their reaction mechanism. Such investigations in the fields of hydrogen evolution nowadays offer ample proof of the use of quantum chemistry as a predictive tool and as an essential component in the understanding of the natural system and in the design of novel synthetic catalysts.

3.2. Geometric structures

The complexity of hydrogenases and the various limitations pertaining to their experimental characterization have fuelled great interest in applying theoretical methods to investigate the structures of models of the different redox states of HG. Looking at the structural aspect of the hydrogenases, theoretical tools have been successfully employed to model both the models and the enzymes. It is now accepted that geometries can be reliably predicted by DFT methods and converge quickly with basis set size, making such prediction rather economical. Long experience has established that the cluster approach using relatively small models (for example, up to ca. 200 atoms) of the protein active sites can provide meaningful mechanistic insights like hydrogen evolution by HG (Figure 12).[53, 54] On the other hand, realistic modelling of the protein environment is achieved by quantum mechanics/molecular mechanics (QM/MM) and “Big QM” approaches. In the case of the hydrogenases, many studies employing these approaches have been reported over the years and contributed to understanding the enzymatic environment and the reaction channels of hydrogenases.[226, 232] In the case of the [NiFe] HG, QM/MM geometry optimizations have contributed to the interpretation of data from crystallography by identifying likely positions of transient H atoms.

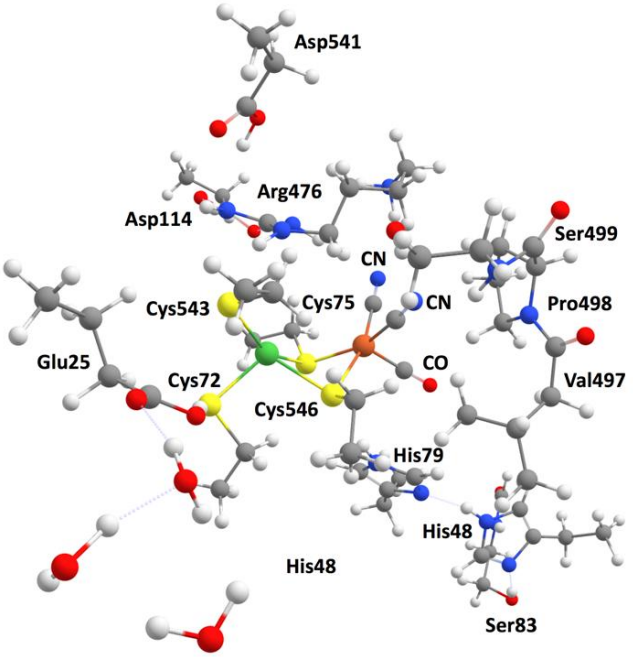

Figure 12. Example of a large model system including relevant amino acids and mimicking the active site of the [NiFe] hydrogenase.

Computational studies have identified the heterolytic cleavage of H_2 as the initial step of the reaction and determined that one hydrogen becomes a bridging hydride whereas the other is accommodated as a proton on one of the cysteine residues.[233, 234] For [FeFe] hydrogenase, QM/MM studies have been extensive and multifaceted. For example, it was shown that the inclusion of two [4Fe4S] clusters in the QM part in addition to the H-cluster provided useful insights into the oxidation states of the active site and the interplay between the two cubanes.[235-237] We can also cite alternative approaches such as the quantum refinement approach based on accurate DFT calculations that was applied to the [FeFe] enzyme to elucidate the nature of the dithiolate ligand.[238]

Molecular dynamics studies have offered support for a proton transport channel to facilitate substrate and product delivery in both hydrogenases.[239] A specific pathway was recently suggested for the second proton, whereby reduction of the active site triggers a structural change, opening a water channel with favourable energetics for the second proton transfer in the [FeFe] HG.[240] In addition, a glutamic residue near the active site was shown to be important for proton transport as its mutation results in loss of activity of [NiFe] hydrogenase.[241] Molecular dynamics can be also combined to other approaches like the coarse-grained (CG) analysis in order to probe important catalytic steps of [FeFe]-hydrogenase, including the transport of electrons to the active site via the iron-sulfur clusters.[242]

Population analysis schemes are simple yet valuable tools, as recently proven by a study using conceptual DFT and Natural Bond Order (NBO) to get new insight regarding the transformation of a proton into a hydride during the catalytic cycle of the [NiFe] HG. Their results indicated that such a transformation is driven by

This journal is © The Royal Society of Chemistry 20xx

Please do not adjust margins

Please do not adjust margins

spontaneous rearrangements of the electron density at room temperature.[243] Such analysis can be very informative about the ligand binding mode and strength to the metal centers of the [FeFe] active site. For instance, a recent report showed that, upon reduction, the distal iron is favoured by the bridging carbonyl which suggests that electrostatic stabilization would influence the charge accumulation occurring prior to H_2 release.[244] Topological analyses based on NBO were also used to revisit the nature and strength of the hydride and dihydrogen interaction with the iron center in the [Ni-Fe] enzyme.[245]

3.3. Electronic structures

Deciphering the spin states of the species that are involved in the catalytic cycle of hydrogenases has reached a whole new level with recent studies showing that it is now possible to conduct calculations with accurate wave function quantum chemical methods, such as the coupled cluster method with single, double and perturbative triple excitations, CCSD(T), and multireference approaches (CASSCF, DMRG). These new advances are very important as energies for reactions involving two-electron transfers to the metal centers like in hydrogenases can be sensitive to the nature of the DFT functional and higher-level methods are thus necessary to obtain more reliable energies and reaction pathways. For example, multi-reference Møller-Plesset[246] and CAS-PT2 calculations[247] were conducted on the active site of the [NiFe] hydrogenase and helped to assign the ground spin state as a singlet through the evaluation of singlet-triplet energy splitting. Wave function methods including CCSD(T) and DMRG have been employed to investigate the interaction of dihydrogen with the [NiFe] active site. These calculations showed that H_2 binds more favourably the Ni site in the singlet state and provided additional understanding about how the active site behaves in the presence of H_2.[248] A similar work based on multiconfigurational short-range DFT calculations supported this conclusion.[249] DMRG has also been applied to study the electronic structure of [4Fe-4S] clusters relevant to the description of the hydrogenase active sites[125] and demonstrated the importance of developing sophisticated methods for electronic structure calculations for an accurate evaluation of the low-lying states that have implications for the reactivity of most bioinorganic systems.

A different aspect of spin-state energetics is found with magnetically interacting (exchange-coupled) transition metal ions as in the case of the [FeFe] hydrogenase whose active site, the H-cluster, corresponds to a [2Fe] subunit coupled to a [4Fe4S] cluster. Such systems can be handled within the DFT framework using the broken-symmetry (BS) approach, which gives access to exchange coupling constants and hence magnetic spin states and energies. Several studies have been reported using this approach showing its capability to provide useful insight on the electronic configuration of the complicated [FeFe] active site by revealing the distribution of metal valences and spin-coupling schemes for the iron–sulfur clusters.[250-252] Similar studies were conducted in the case of the O_2-tolerant [NiFe] hydrogenases that contain a proximal [4Fe-3S] cluster whose redox states and magnetic couplings were elucidated and discussed using BS-DFT calculations.[253-255]

3.4. Spectroscopic properties

In conjunction with experimental methods, theoretical calculations appear as an invaluable tool for the interpretation of spectroscopic results. Spectroscopic data for a sufficiently complex system rarely have a unique interpretation in terms of electronic structure. On the other hand, it can be difficult or impossible to identify the most appropriate electronic structure description using only total energies as criterion in quantum chemical studies. Therefore, the explicit calculation of spectroscopic properties is the way toward a better understanding and more reliable verification of the geometric and electronic structures of a complex system that is being modeled. Spectroscopic techniques including FT-IR, Nuclear resonance vibrational spectroscopy (NRVS), Electron Paramagnetic Resonance (EPR) or Mossbauer have been widely employed to investigate [NiFe] and [FeFe] enzymes and models, and often combined with theoretical methods (Figure 13).[29]

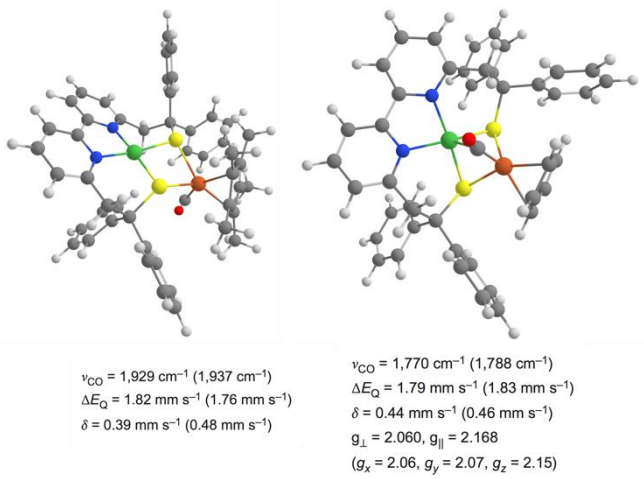

Figure 13. Structures of the biomimetic models for the Ni-SIa (a) and Ni-L (b) states of the [NiFe] hydrogenase identified by combining spectroscopic measurements and DFT computations. Adapted with permission from Ref. 40. Copyright 2016 Nature Publishing Group.

Following the development of a computational methodology for an accurate prediction of the IR spectra of the active site of [FeFe]-hydrogenase,[256] many studies have been conducted using DFT calculations and helped in the unambiguous assignment of the structure and redox states of intermediates like for the H-cluster.[257-260] While the calculated absolute vibrational frequencies are often not quantitatively accurate, shifts in frequencies due to protonation and/or reduction events are reliable. Due to the peculiar vibrational frequencies of the CN and CO groups, it is possible to distinguish the redox states of the [NiFe] active site. Indeed, the stretching frequencies of these ligands are spectroscopic fingerprints that can probe the electronic structure of the metal core and the structural composition of the active site.[261] Comparison between computed and experimental vibrational frequencies can provide even more subtle information like the influence of the second coordination sphere on the electronic structure of the [NiFe] active site.[262] A

Please do not adjust margins

Please do not adjust margins

review article recently highlighted that the correlation between experimental and DFT-calculated IR spectra is a powerful tool to identify some key features of the active site cofactor of HG and to unravel the structure of transient intermediates with great precision.[227]

NRVS is emerging as spectroscopic technique to study hydrogenases. The vibrational density of states spectra that are obtained when using NRVS can be reliably predicted using density functional theory (DFT) and assists in spectral assignments. A striking example comes from a recent study that combined IR and NRVS spectroscopic techniques to DFT calculations to elucidate the structures and the local coordination spheres of the one and two-electron reduced intermediates of the [FeFe] HG. Their results showed no evidence for a bridging hydride which may have important consequences for the mechanism of H_2 conversion by this enzyme.[263] In a similar manner, the NRVS spectroscopy was employed together with DFT calculations to identify one catalytic state of the [FeFe] hydrogenase, providing decisive information regarding H_2 bond formation by the enzyme. This study was conducted on an [FeFe] HG using NRVS experiments in conjunction with DFT calculations and showed that H_{hyd} is the catalytic state one step prior H_2 formation[264] while another report studying an [FeFe] variant elucidated the bending modes of the terminal Fe-H species,[265] both providing mechanistic insight into the reaction coordinate for H_2 bond formation by [FeFe]-hydrogenases. Similar studies were also conducted on [NiFe] enzymes and enabled the distinct observation of Fe–CN and Fe–CO bending and stretching modes for the active sites in [NiFe] HG[266, 267] while a recent report showed the direct evidence for a hydride bridge in the active site of the fully reduced Ni-R form whose electronic structure could be assigned as a low-spin $Ni^{II}(\mu\text{-}H)Fe^{II}$ core.[268]

EPR spectroscopic techniques have been demonstrated as extremely useful to investigate paramagnetic intermediate states during hydrogen conversion catalytic cycle.[228] Understanding the hydrogenase mechanism implies being able to determine the exact structure of the active site and its surrounding for all states. In addition to this information, EPR spectroscopy can also give access to the oxidation and spin states of the metal ions involved and their interaction with each other or with the ligand sphere. One known example of the use of theoretical EPR spectroscopy to study HG deals with the Ni-L state, detected when the Ni-C state is put under illumination. DFT calculations were conducted on all possible structures of Ni-L state and g tensors together with hyperfine coupling constants were computed as indicators to compare with EPR data. From the calculated spectroscopic parameters, it was proposed that the proton most likely binds to the terminal cysteines rather than the bridging ones and that a metal–metal bond between nickel and iron was present.[269] Another example lies in the study of an artificial [FeFe] hydrogenase for which DFT calculations helped to determine the structure of the active site. Specially, computation of the hyperfine coupling constants reproduced experimental data and highlighted the presence of a CN ligand with the cyanide C atom bridging one mixed-valent iron of the [4Fe4S] cluster and the N atom bound to one iron of the binuclear unit.[270] Several experimental and theoretical investigations of the H-cluster using advanced pulsed EPR techniques and DFT calculations have been carried out. They showed that spin polarization in the dtma ligand can be linked to the asymmetric coordination of the distal iron site with its terminal CN^- and CO ligands which would have implication on stabilizing the iron-hydride intermediate in the catalytic cycle.[271] More recently, EPR data together with DFT calculations clearly showed that a specific conformation of the external CO ligand is favoured so that it binds in an apical position on the iron center. These combined studies highlighted the rigid configuration of the CO and CN ligands which is stabilized by H-bonds and has implication on the reactivity of the enzyme as it ensures minimal reorganization energy during catalysis.[272]

As an indispensable analytical tool in iron coordination chemistry, Mössbauer spectroscopy is a valuable spectroscopic technique to study hydrogenases. It can probe the spin state of the metal centers in the active sites as well as their local environment like the coordination geometry. For instance, theoretical Mossbauer spectroscopy has been used to investigate the [4Fe3S] cluster proximal to the active site of the O_2 tolerant [NiFe] HG. The calculated isomer shifts and quadrupole splitting helped in discriminating between different interpretation of the data and a clear assignment of both the spin coupling scheme and the redox states within the iron-sulphur cluster was made possible.[273] Combined with theoretical calculations, this spectroscopic technique has been also employed to study diverse [FeFe] hydrogenase intermediates. The putative structures of these intermediates were obtained from QM/MM calculations and the comparison between calculated and experimental isomer shifts could be used to discriminate between different intermediates following a proper calibration based on iron-based model systems.[274] The same approach was also used for studying the coordination environment of an active site model complex. Based on the calculated isomer shifts and quadrupole splitting, they could determine the protonation states, the presence of a bound water and the redox state of the iron center providing meaningful insight regarding the proton transfer mechanism.[275] A more recent study made use of several techniques including Mössbauer spectroscopy and DFT calculations to set-up structure-property relationships and to show how that the reactivity of all HG enzymes could be mimicked using isomers of a [NiFe] bio-inspired model.[276]

With the recent development of dedicated quantum chemistry program packages[277-280] the use of theoretical spectroscopy has been democratized with the aim to connect the results of computations to experimental observables since spectroscopic properties remain a precise and sensitive fingerprint of the electronic structure for a given system. Consequently, combining spectroscopic characterizations with theoretical calculations has been successfully employed by many research groups to identify the geometric and electronic structures of biomimetic[40, 60, 265, 268, 281-283] and bio-inspired[284-290] models of hydrogenases and appears as a prerequisite to any further computational investigation of their reactivity towards H_2 evolution.

This journal is © The Royal Society of Chemistry 20xx

Please do not adjust margins

Please do not adjust margins

3.5. Thermodynamics

Studying the reactivity of hydrogenases and related model systems implies the initial determination of thermodynamic properties like redox potentials and pK_a values. Indeed, the hydrogen evolution reaction proceeds via the transfer of two electrons and two protons to form H_2. For a given catalyst, six sequences can be formally considered: ECEC, ECCE, EECC, CCEE, CEEC and CECE with E being the electrochemical event i.e. the electron transfer step and C being the chemical event i.e. the proton transfer step (Figure 14). Through the computational evaluation of the free energies of the species associated to these chemical and electrochemical steps, it is possible to get access to the thermodynamic quantities with a reasonably high level of accuracy. The theoretical prediction of these parameters is usually conducted using Born−Haber cycle and the calculated Gibbs free energy change associated with the reduction and protonation event in solution, respectively. To calculate experimentally relevant electrochemical quantities, reference systems have to be considered. To do so, the absolute reduction potential of the reference electrode and the pK_a of the acid serving as the proton source have to be computed and further subtracted from the Gibbs free energy change in solution for reduction and protonation.[229, 291]

Electronic structure methods have extensively used to predict relative redox potentials and pK_a values of molecular electrocatalysts and hydrogenases models as a first step for further mechanistic investigations.[33, 226, 231, 287, 292, 293]

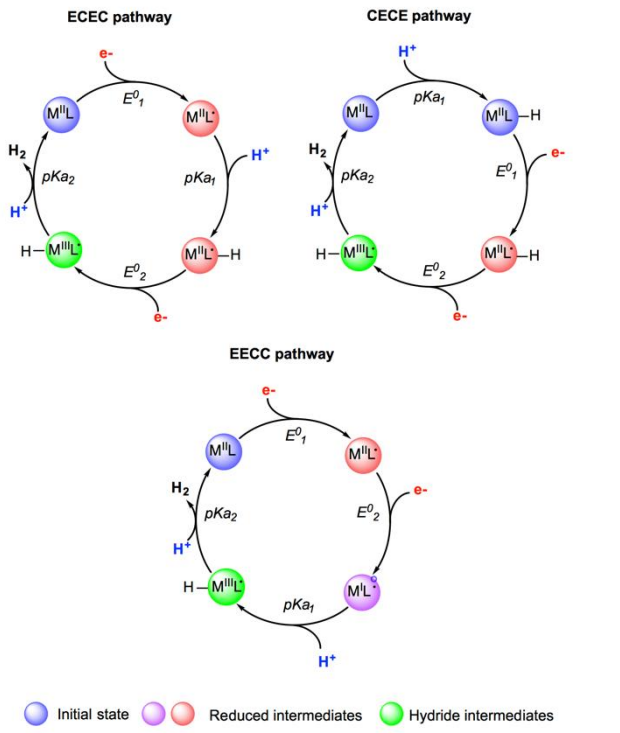

Figure 14. Selected examples of sequences and putative intermediates considered during hydrogen evolution reaction. Adapted with permission from Ref. 291. Copyright 2019 Chem Pub Soc.

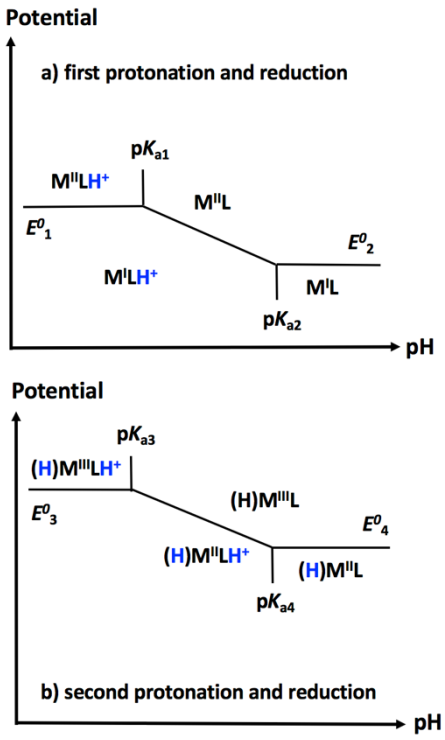

Figure 15. Representation of the Pourbaix diagram of a given catalyst based on a CECE sequence with MLH the ligand protonated species and (H)M the hydride intermediates. The horizontal lines are plotted with respect to the reduction potentials of the catalyst, while vertical lines are plotted for its pKa values. Diagonal lines separate processes involving a simultaneous oxidation and protonation process.

One useful tool for envisioning the relationship between E and C steps during hydrogen evolution finally lies in the construction of Pourbaix diagrams. These diagrams depict the thermodynamically most stable species for a given reduction potential and pH value (Figure 15). For a given catalyst, constructing a theoretical Pourbaix diagram allows to evaluate the stability of all possible intermediate species on a broad pH range. Linear correlations using Pourbaix diagrams, redox potentials and pK_a values have been established for cobalt and nickel electrocatalysts as powerful tools in catalyst design, enabling the computational prediction of properties for electrocatalysts that have not yet been synthesized.[292, 294-296]

3.6. Reaction mechanisms

Computational approaches have been widely used to elucidate various mechanistic aspects of catalytic hydrogen evolution, including possible protonation sites, energetics of distinct pathways, order of steps, and stepwise versus concerted processes. The reliable calculation of relative stabilities of various isomeric forms and the detailed insight into plausible pathways for their interconversion are crucial to address reactivity problems in hydrogenase chemistry. Using DFT methods, free energy profiles of possible mechanistic routes can be evaluated along with the corresponding intermediates and transition states resulting from reduction and/or protonation events. The theoretical determination of the quantities associated to the electrochemical and chemical

Please do not adjust margins

Please do not adjust margins

steps was shown to help to determine which pathway is favoured among all possible sequences. Many studies made use of detailed DFT calculations to inspect free energy landscapes and to identify the predominant pathway for proton reduction among all possible sequences in the case of molecular electrocatalysts[61, 62, 292, 294, 297-309] and hydrogenase models (Figure 16).[39, 59, 281, 282, 287, 288, 310-316]

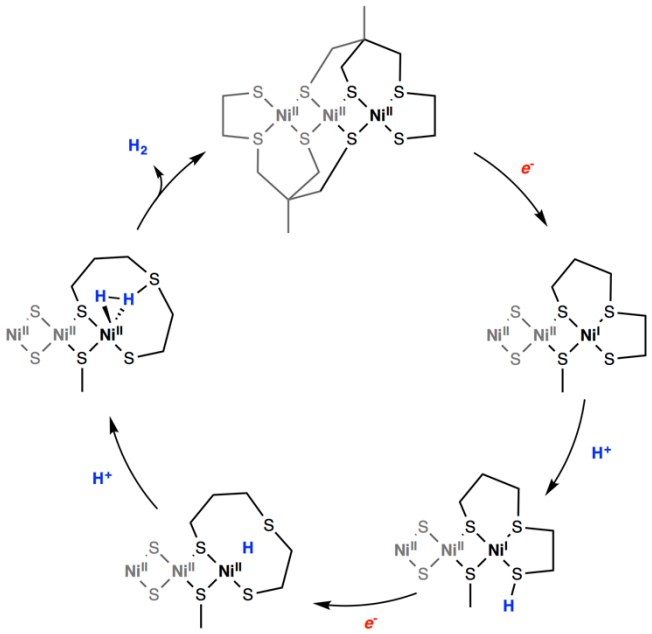

Figure 16. DFT computed reaction mechanism for hydrogen evolution mediated by a bio-inspired mimic for the [Ni-Fe] hydrogenase. Adapted with permission from Ref. 299. Published by The Royal Society of Chemistry.

Environmental effects play an important role in modulating the energetics of every intermediate state in the reaction pathway of HER catalysts. Specially, the presence of solvent molecules or anions from the acid serving as the proton source can play a crucial role in modulating the kinetic and thermodynamic aspects of the reaction.[317] For instance, the proton source can affect the thermodynamics of catalytic event and a theoretical description of these effects on the pKa value, metal redox states or protonation states are necessary to inspect the feasibility of different pathways for the catalytic cycle of cobalt catalysts.[293, 318] The DFT investigation of a nickel catalyst reported the effect of the solvent on redox properties and how it can affect the stability of the metal oxidation state by changing its coordination. In this study, accurate estimates of redox potentials could be estimated by accounting for a possible ligand release.[296] The importance of the anation was demonstrated in a recent DFT study on a cobalt catalyst which showed that substitution of a bound acetonitrile with acetate alters the proton reduction energetics (Figure 17).[317] Thus, accounting for these effects and the possible direct involvement of the solvent are critical considerations in computational studies.

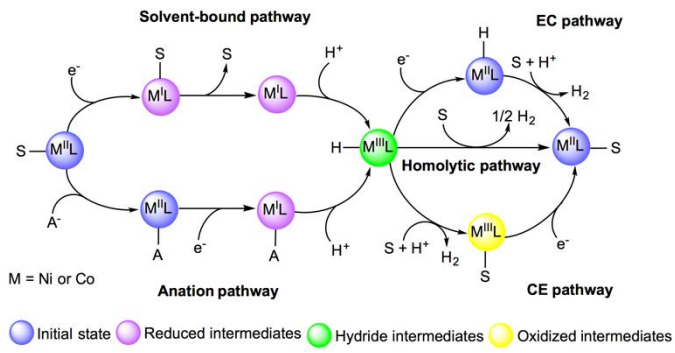

Figure 17. Examples of solvent-bound and anation reaction pathways to form hydride intermediates. Adapted with permission from Ref. 291. Copyright 2019 Chem Pub Soc.

For a complete rationalization of the reactivity towards hydrogen evolution, it is often sufficient to evaluate the activation barrier for thermally activated processes. For other cases, free energies of reactions have to be combined with kinetic rates (Figure 18). To do so, the rate constants for proton transfer, electron transfer, and concerted events have to be calculated as the kinetics of these various steps can play an important role in the reaction pathways. Such an estimate requires further analysis, involving accurate evaluation of reorganization energies, adiabatic couplings for electron transfer, and methods that can properly sample the quantum dynamics of proton-coupled electron transfer. Several studies on molecular electrocatalysts have reported the theoretical evaluation of electrochemical non-adiabatic rate constants for electron and proton transfer within the Marcus theory framework.[229, 319-321] In the case of hydrogenases, kinetic rates have proven hard to extract.[322] However, combining MD data with phenomenological rate equations, hydrogen diffusion constants in HG were recently calculated and found to be in agreement with experiments.[323, 324]

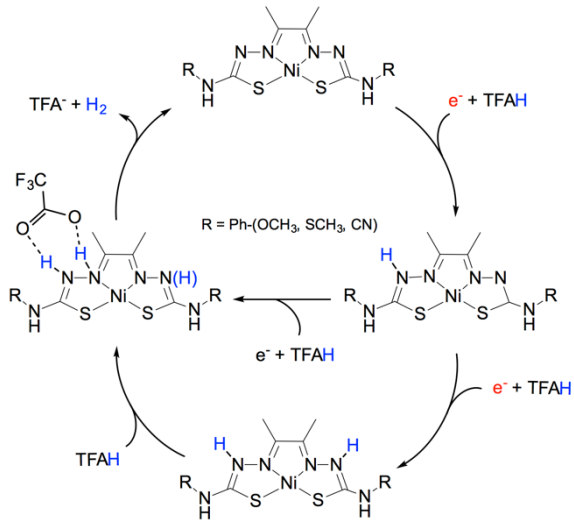

Figure 18. DFT computed reaction mechanism for hydrogen evolution mediated by a molecular catalyst highlighting the influence of the proton source on the preferable pathway. Adapted with permission from Ref. 309. Published by The Royal Society of Chemistry.

This journal is © The Royal Society of Chemistry 20xx

Please do not adjust margins

Please do not adjust margins

Computational studies on the mechanistic aspects of hydrogen evolution by hydrogenases have been an active topic of research in many groups.[224, 291, 325, 326] For instance, various computational works have been performed to study the reaction cycle of the [NiFe] HG with a special emphasis on H_2 binding site and proton binding position.[233, 234, 327, 328] While there has not being a complete consensus on the catalytic cycle (Figure 10), the mechanism presumably starts with the Ni−SI_a state binding H_2 on the Ni^{II} site. H_2 is heterolytically cleaved yielding the Ni-R state displaying a hydride bound to both two metals and a proton binding the Cys546. The next step involves two possibilities, depending on whether a proton or an electron is removed first. Both scenario lead to the formation of the Ni-C intermediate featuring a Ni^{III} center. Subsequently, the formed hydride is oxidized, the metal reaches its Ni^{I} state, and the resulting proton is transferred to Cys546. The cycle is then completed with the formation of the Ni-SI_a resting state. The reaction mechanism of H_2 oxidation by [NiFe] hydrogenase was recently revised using DFT methods and focused on the energetics of the entire catalytic cycle. Here two different mechanisms were investigated: the heterolytic cleavage of H_2 and the homolytic one that occur with different redox states of the [NiFe] core. Their main finding is that reaching the homolytic mechanism implies one cycle of the heterolytic mechanism. They also correlated the design of the [NiFe] active site complex to the criteria of energy minimization upon proton and electron release, and thus observed an endergonic binding of H_2 which has direct implications on the development of efficient HG mimics.[329, 330] Another study using DFT calculations recently reported new mechanistic insights on the reactivation process involving oxidized forms of the [NiFe] HG. While [FeFe]-hydrogenases are irreversibly inactivated by O_2, [NiFe] are more resistant to oxidation. However, oxygen exposure creates a mixture of two inactive, oxidized forms, the Ni−B and Ni−A states. Importantly, these are not permanently inactivated but can be reactivated by reduction. The results of this study showed that the bridging hydroxide ligand found in the two states is lost upon reduction and protonation steps at the active site. Structures for the species obtained upon reduction of Ni-A and Ni-B were proposed and specific structural features were shown to impact the reactivation kinetics of the oxidized and inactive states.[331]

Similarly, with [NiFe] hydrogenases, distinct mechanisms were proposed for the [FeFe] ones and differ mainly in the protonation sites and H_2 binding. Lately, computational studies together with experimental investigations seem consistent with one scenario. When considering the catalytic cycle in the direction of H_2 production (Figure 11), the [FeFe]-hydrogenase state directly involved in hydrogen binding is H_{ox}. In this state, the redox of the H-cluster can formally be described as $Fe^{II}Fe^{I}$. One electron reduction and protonation of H_{ox} yields a transient $Fe^{I}Fe^{I}$ species featuring a protonated dtma ligand and referred as H_{red}. Further proton-electron transfer takes place resulting in the formation of H_{hyd}, a mixed-valence $Fe^{I}Fe^{II}$ species featuring a terminal hydride ligand and a protonated amine. H_2 detachment from this intermediate brings the H-cluster back to the initial $Fe^{II}Fe^{I}$ redox state.[332-335] The catalytic activation of H_2 by [FeFe] HG has been recently revised by means of DFT methods to elucidate the specific details underlying the different performances of the enzymes when compared to biomimetic models. Their results highlighted that the enzyme performs better which can be correlated with two requisites: (i) the presence of an electron-poor iron center which favors H_2 binding and (ii) a electron- rich cofactor which ensures oxidation of the metal–H_2 adduct. Disclosure of these differences will guide the development of novel biomimetic models and lead to reconsider the utility of CN ligand in the catalyst design.[336]

In addition to the extensive use of DFT methods, QM/MM thermodynamic cycle perturbation (QTCP) computations were recently shown as a valuable approach to obtain accurate free energies to model the catalytic cycle for hydrogen evolution by hydrogenases. In these calculations, the QM/MM method is used to compute the energy differences on configurations generated by MD simulations. QTCP currently gives access to reaction energies with an accuracy of 20 $kJ.mol^{-1}$. Reaching higher degree of precision will require, among other things, to take into account other factors like polarization or short-range electrostatics and the development of high-level methods, both being the topic of intense research efforts.[233, 234, 337, 338]

4. Conclusions

Impressive advances have been made in recent years in understanding the structure and function of the photosynthetic oxygen-evolving complex and of hydrogenases. Quantum chemistry has played a key role in most of these efforts, especially when it has been fruitfully combined with experiment. Nevertheless, photosystem II and the hydrogenases continue to pose great challenges, both in terms of fundamental understanding and in terms of the technical difficulties involved in studying them. In the field of water oxidation an incredible amount of insight has been gained on the geometric and electronic structure of the oxygen-evolving complex, yet serious questions remain open regarding the precise nature of several catalytic intermediates and nothing is known with certainty about the critical dioxygen formation and evolution steps. In the field of hydrogen evolution, despite the recent advances made in the understanding of the mechanism by which hydrogenases exert their function, especially the formation of hydride species or the key role of the metal site involved in catalysis, many essential aspects of the catalytic process including CO/O_2 inhibition or activation/deactivation processes are incompletely understood. From the point of view of quantum chemistry both more accurate methods and more reliable models will be needed to retain the pace of theory-led discovery in the field of metalloenzyme solar fuel research. Among the points highlighted in this article is the development of first principles electronic structure methods that overcome deficiencies associated with existing DFT implementations and deliver accurate predictions of spin-state and reaction energetics for systems containing several interacting open-shell metal ions. Coupled to that will be the more extensive and more reliable use of quantum chemical approaches for the prediction of spectroscopic properties, which is a major

Please do not adjust margins

Please do not adjust margins

point of contact between electronic structure theory and experiment. In terms of model definition, the conventional QM-cluster approach will be increasingly disfavoured over a more complete treatment of the protein environment. This is not a luxury but a necessity: the active site is not a catalyst, the whole enzyme is. The protein matrix is exclusively responsible for critical elements of enzyme function such as electron transfer, regulation of substrate delivery, proton access/egress, product release, etc, therefore our understanding of enzyme function will keep expanding to encompass the functional role of the protein beyond the immediate vicinity of the active sites. A multitude of different methods are emerging to achieve this type of treatment, many of which will in addition be able to offer access to a dynamical view of the system. Computational simulations will increasingly influence our understanding of kinetics related both to the transport of substrates to active sites that are buried within the protein and only accessible via specific channels, and to the release of products. With the broader goal in mind of overcoming the efficiency gap between the biological systems and biomimetic/bio-inspired compounds, the most successful strategy remains to combine insights from both systems to uncover differences as well as common principles that can be put to use in the design of water oxidation and hydrogen evolution catalysts. Computational methods have made tremendous advances to reach the level of utility they have today in this effort, and their contribution in the future is certain to increase.

Conflicts of interest

There are no conflicts to declare.

Acknowledgements

The authors gratefully acknowledge financial support of this work by the French National Research Agency and the Deutsche Forschungsgemeinschaft (CODEC, ANR-19-CE05_0030_01; NiFemim, ANR-DFG-2016-NLE), from the France–Germany Hubert Curien Program – German Academic Exchange Service (DAAD) (Procope 2019-2020 project 42525PB / DAAD project 57445526), and from the Max Planck Society.

This journal is © The Royal Society of Chemistry 20xx

Please do not adjust margins

Please do not adjust margins

Authors

Maylis Orio was born in 1981. She obtained her PhD in Chemistry from the University of Grenoble in 2007. She is a CNRS researcher from Aix-Marseille University. Her research interests focus on the use of quantum bioinorganic chemistry in relation with catalysis, including in the field of hydrogen production.

Dimitrios A. Pantazis was born in 1976. He obtained his PhD in Chemistry from the University of York and is currently a research group leader at the Max-Planck-Institut für Kohlenforschung. His research interests focus on quantum bioinorganic chemistry and computational spectroscopy in relation to all aspects of natural and artificial photosynthesis.

References

1. A. Borgschulte, *Frontiers in Energy Research*, 2016, **4**.
2. J. Barber, *Chem. Soc. Rev.*, 2009, **38**, 185-196.
3. T. R. Cook, D. K. Dogutan, S. Y. Reece, Y. Surendranath, T. S. Teets and D. G. Nocera, *Chem. Rev.*, 2010, **110**, 6474-6502.
4. W. Lubitz and W. Tumas, *Chem. Rev.*, 2007, **107**, 3900-3903.
5. N. Cox, D. A. Pantazis, F. Neese and W. Lubitz, *Interface Focus*, 2015, **5**, 20150009.
6. J. Barber and P. D. Tran, *J. R. Soc. Interface*, 2013, **10**, 20120984.
7. W. Lubitz, E. J. Reijerse and J. Messinger, *Energy Environ. Sci.*, 2008, **1**, 15-31.
8. J. Messinger, W. Lubitz and J.-R. Shen, *Phys. Chem. Chem. Phys.*, 2014, **16**, 11810-11811.
9. D. Kim, K. K. Sakimoto, D. Hong and P. Yang, *Angew. Chem., Int. Ed.*, 2015, **54**, 3259-3266.
10. M. E. El-Khouly, E. El-Mohsnawy and S. Fukuzumi, *J. Photochem. Photobiol., C*, 2017, **31**, 36-83.
11. B. Zhang and L. Sun, *Chem. Soc. Rev.*, 2019, **48**, 2216-2264.
12. D. Gust, T. A. Moore and A. L. Moore, *Acc. Chem. Res.*, 2009, **42**, 1890-1898.
13. D. G. Nocera, *Acc. Chem. Res.*, 2012, **45**, 767-776.
14. Y. Tachibana, L. Vayssieres and J. R. Durrant, *Nat. Photonics*, 2012, **6**, 511-518.
15. R. E. Blankenship, *Molecular Mechanisms of Photosynthesis*, Wiley, Chichester, 2nd edn., 2014.
16. V. Krewald, M. Retegan and D. A. Pantazis, *Top. Curr. Chem.*, 2016, **371**, 23-48.
17. D. A. Pantazis, *ACS Catal.*, 2018, **8**, 9477-9507.
18. S. Paul, F. Neese and D. A. Pantazis, *Green Chem.*, 2017, **19**, 2309-2325.
19. C. Zhang, C. Chen, H. Dong, J.-R. Shen, H. Dau and J. Zhao, *Science*, 2015, **348**, 690-693.
20. C. Chen, Y. Li, G. Zhao, R. Yao and C. Zhang, *ChemSusChem*, 2017, **10**, 4403-4408.
21. Y. Li, R. Yao, Y. Chen, B. Xu, C. Chen and C. Zhang, *Catalysts*, 2020, **10**, 185.
22. J. S. Kanady, E. Y. Tsui, M. W. Day and T. Agapie, *Science*, 2011, **333**, 733-736.
23. Z. Han, K. T. Horak, H. B. Lee and T. Agapie, *J. Am. Chem. Soc.*, 2017, **139**, 9108-9111.
24. H. B. Lee, A. A. Shiau, P. H. Oyala, D. A. Marchiori, S. Gul, R. Chatterjee, J. Yano, R. D. Britt and T. Agapie, *J. Am. Chem. Soc.*, 2018, **140**, 17175-17187.
25. H. B. Lee, D. A. Marchiori, R. Chatterjee, P. H. Oyala, J. Yano, R. D. Britt and T. Agapie, *J. Am. Chem. Soc.*, 2020, **142**, 3753-3761.
26. P. Kurz, *Top. Curr. Chem.*, 2016, **371**, 49-72.
27. M. M. Najafpour, G. Renger, M. Hołyńska, A. N. Moghaddam, E.-M. Aro, R. Carpentier, H. Nishihara, J. J. Eaton-Rye, J.-R. Shen and S. I. Allakhverdiev, *Chem. Rev.*, 2016, **116**, 2886-2936.
28. J. D. Blakemore, R. H. Crabtree and G. W. Brudvig, *Chem. Rev.*, 2015, **115**, 12974-13005.
29. W. Lubitz, H. Ogata, O. Rudiger and E. Reijerse, *Chem. Rev.*, 2014, **114**, 4081-4148.
30. M. Y. Darensbourg and W. Weigand, *Eur. J. Inorg. Chem.*, 2011, **2011**, 917-918.
31. R. K. Thauer, *Eur. J. Inorg. Chem.*, 2011, **2011**, 919-921.
32. P. Vashi, *Eur. J. Inorg. Chem.*, 2011, **2011**, 915-916.
33. D. Schilter, J. M. Camara, M. T. Huynh, S. Hammes-Schiffer and T. B. Rauchfuss, *Chem. Rev.*, 2016, **116**, 8693-8749.
34. T. R. Simmons, G. Berggren, M. Bacchi, M. Fontecave and V. Artero, *Coord. Chem. Rev.*, 2014, **270-271**, 127-150.
35. T. B. Rauchfuss, *Acc. Chem. Res.*, 2015, **48**, 2107-2116.
36. M. Y. Darensbourg, E. J. Lyon and J. J. Smee, *Coord. Chem. Rev.*, 2000, **206-207**, 533-561.
37. M. E. Carroll, B. E. Barton, T. B. Rauchfuss and P. J. Carroll, *J. Am. Chem. Soc.*, 2012, **134**, 18843-18852.
38. Z. Li, Y. Ohki and K. Tatsumi, *J. Am. Chem. Soc.*, 2005, **127**, 8950-8951.
39. S. Canaguier, M. Field, Y. Oudart, J. Pécaut, M. Fontecave and V. Artero, *Chem. Commun.*, 2010, **46**, 5876-5878.
40. D. Brazzolotto, M. Gennari, N. Queyriaux, T. R. Simmons, J. Pécaut, S. Demeshko, F. Meyer, M. Orio, V. Artero and C. Duboc, *Nat. Chem.*, 2016, **8**, 1054-1060.
41. Y. Ohki, K. Yasumura, M. Ando, S. Shimokata and K. Tatsumi, *Proc. Natl. Acad. Sci. U. S. A.*, 2010, **107**, 3994-3997.
42. O. T. Holton and J. W. Stevenson, *Platinum Metals Review*, 2013, **57**, 259-271.
43. J. R. McKone, S. C. Marinescu, B. S. Brunschwig, J. R. Winkler and H. B. Gray, *Chem. Sci.*, 2014, **5**, 865-878.
44. M. L. Helm, M. P. Stewart, R. M. Bullock, M. R. DuBois and D. L. DuBois, *Science*, 2011, **333**, 863-866.
45. M. Razavet, V. Artero and M. Fontecave, *Inorg. Chem.*, 2005, **44**, 4786-4795.
46. V. Artero and J.-M. Saveant, *Energy Environ. Sci.*, 2014, **7**, 3808-3814.
47. S. Cherdo, S. E. Ghachtouli, M. Sircoglou, F. Brisset, M. Orio and A. Aukauloo, *Chem. Commun.*, 2014, **50**, 13514-13516.
48. M. Beyler, S. Ezzaher, M. Karnahl, M.-P. Santoni, R. Lomoth and S. Ott, *Chem. Commun.*, 2011, **47**, 11662-11664.
49. J. L. Dempsey, B. S. Brunschwig, J. R. Winkler and H. B. Gray, *Acc. Chem. Res.*, 2009, **42**, 1995-2004.
50. N. Kaeffer, M. Chavarot-Kerlidou and V. Artero, *Acc. Chem. Res.*, 2015, **48**, 1286-1295.
51. X. Hu, B. S. Brunschwig and J. C. Peters, *J. Am. Chem. Soc.*, 2007, **129**, 8988-8998.
52. C. J. Cramer and D. G. Truhlar, *Phys. Chem. Chem. Phys.*, 2009, **11**, 10757-10816.
53. M. R. A. Blomberg, T. Borowski, F. Himo, R.-Z. Liao and P. E. M. Siegbahn, *Chem. Rev.*, 2014, **114**, 3601-3658.
54. F. Himo, *J. Am. Chem. Soc.*, 2017, **139**, 6780-6786.
55. R. Lonsdale, J. N. Harvey and A. J. Mulholland, *Chem. Soc. Rev.*, 2012, **41**, 3025-3038.
56. F. Neese, *Coord. Chem. Rev.*, 2009, **253**, 526-563.
57. H. M. Senn and W. Thiel, *Angew. Chem., Int. Ed.*, 2009, **48**, 1198-1229.
58. K. Weber, T. Krämer, H. S. Shafaat, T. Weyhermüller, E. Bill, M. van Gastel, F. Neese and W. Lubitz, *J. Am. Chem. Soc.*, 2012, **134**, 20745-20755.
59. S. Ding, P. Ghosh, A. M. Lunsford, N. Wang, N. Bhuvanesh, M. B. Hall and M. Y. Darensbourg, *J. Am. Chem. Soc.*, 2016, **138**, 12920-12927.

Please do not adjust margins

Please do not adjust margins

60. L. Wang, M. Gennari, A. Barrozo, J. Fize, C. Philouze, S. Demeshko, F. Meyer, M. Orio, V. Artero and C. Duboc, *ACS Catal.*, 2019, **10**, 177-186.
61. T. Straistari, J. Fize, S. Shova, M. Réglier, V. Artero and M. Orio, *ChemCatChem*, 2017, **9**, 2262-2268.
62. T. Straistari, R. Hardré, J. Fize, S. Shova, M. Giorgi, M. Réglier, V. Artero and M. Orio, *Chem. Eur. J.*, 2018, **24**, 8779-8786.
63. C. Greco, G. Zampella, L. Bertini, M. Bruschi, P. Fantucci and L. De Gioia, *Inorg. Chem.*, 2007, **46**, 108-116.
64. A. Sirohiwal, F. Neese and D. A. Pantazis, *J. Am. Chem. Soc.*, 2020, **142**, 18174-18190.
65. T. Cardona, A. Sedoud, N. Cox and A. W. Rutherford, *Biochim. Biophys. Acta Bioenerg.*, 2012, **1817**, 26-43.
66. A. W. Rutherford, A. Osyczka and F. Rappaport, *FEBS Lett.*, 2012, **586**, 603-616.
67. R. Croce and H. van Amerongen, *Nat. Chem. Biol.*, 2014, **10**, 492-501.
68. A. Klauss, M. Haumann and H. Dau, *Proc. Natl. Acad. Sci. U. S. A.*, 2012, **109**, 16035-16040.
69. V. K. Yachandra, K. Sauer and M. P. Klein, *Chem. Rev.*, 1996, **96**, 2927-2950.
70. A. Zouni, H. T. Witt, J. Kern, P. Fromme, N. Krauss, W. Saenger and P. Orth, *Nature*, 2001, **409**, 739-743.
71. K. N. Ferreira, T. M. Iverson, K. Maghlaoui, J. Barber and S. Iwata, *Science*, 2004, **303**, 1831-1838.
72. B. Loll, J. Kern, W. Saenger, A. Zouni and J. Biesiadka, *Nature*, 2005, **438**, 1040-1044.
73. M. Lundberg and P. E. M. Siegbahn, *Phys. Chem. Chem. Phys.*, 2004, **6**, 4772-4780.
74. E. M. Sproviero, J. A. Gascon, J. P. McEvoy, G. W. Brudvig and V. S. Batista, *J. Chem. Theory Comput.*, 2006, **2**, 1119-1134.
75. Y. Umena, K. Kawakami, J.-R. Shen and N. Kamiya, *Nature*, 2011, **473**, 55-60.
76. M. Suga, F. Akita, K. Hirata, G. Ueno, H. Murakami, Y. Nakajima, T. Shimizu, K. Yamashita, M. Yamamoto, H. Ago and J.-R. Shen, *Nature*, 2015, **517**, 99-103.
77. I. D. Young, M. Ibrahim, R. Chatterjee, S. Gul, F. D. Fuller, S. Koroidov, A. S. Brewster, R. Tran, R. Alonso-Mori, T. Kroll, T. Michels-Clark, H. Laksmono, R. G. Sierra, C. A. Stan, R. Hussein, M. Zhang, L. Douthit, M. Kubin, C. de Lichtenberg, L. Vo Pham, H. Nilsson, M. H. Cheah, D. Shevela, C. Saracini, M. A. Bean, I. Seuffert, D. Sokaras, T.-C. Weng, E. Pastor, C. Weninger, T. Fransson, L. Lassalle, P. Bräuer, P. Aller, P. T. Docker, B. Andi, A. M. Orville, J. M. Glownia, S. Nelson, M. Sikorski, D. Zhu, M. S. Hunter, T. J. Lane, A. Aquila, J. E. Koglin, J. Robinson, M. Liang, S. Boutet, A. Y. Lyubimov, M. Uervirojnangkoorn, N. W. Moriarty, D. Liebschner, P. V. Afonine, D. G. Waterman, G. Evans, P. Wernet, H. Dobbek, W. I. Weis, A. T. Brunger, P. H. Zwart, P. D. Adams, A. Zouni, J. Messinger, U. Bergmann, N. K. Sauter, J. Kern, V. K. Yachandra and J. Yano, *Nature*, 2016, **540**, 453-457.
78. M. Suga, F. Akita, M. Sugahara, M. Kubo, Y. Nakajima, T. Nakane, K. Yamashita, Y. Umena, M. Nakabayashi, T. Yamane, T. Nakano, M. Suzuki, T. Masuda, S. Inoue, T. Kimura, T. Nomura, S. Yonekura, L.-J. Yu, T. Sakamoto, T. Motomura, J.-H. Chen, Y. Kato, T. Noguchi, K. Tono, Y. Joti, T. Kameshima, T. Hatsui, E. Nango, R. Tanaka, H. Naitow, Y. Matsuura, A. Yamashita, M. Yamamoto, O. Nureki, M. Yabashi, T. Ishikawa, S. Iwata and J.-R. Shen, *Nature*, 2017, **543**, 131-135.
79. A. Tanaka, Y. Fukushima and N. Kamiya, *J. Am. Chem. Soc.*, 2017, **139**, 1718-1721.
80. J. Kern, R. Chatterjee, I. D. Young, F. D. Fuller, L. Lassalle, M. Ibrahim, S. Gul, T. Fransson, A. S. Brewster, R. Alonso-Mori, R. Hussein, M. Zhang, L. Douthit, C. de Lichtenberg, M. H. Cheah, D. Shevela, J. Wersig, I. Seuffert, D. Sokaras, E. Pastor, C. Weninger, T. Kroll, R. G. Sierra, P. Aller, A. Butryn, A. M. Orville, M. Liang, A. Batyuk, J. E. Koglin, S. Carbajo, S. Boutet, N. W. Moriarty, J. M. Holton, H. Dobbek, P. D. Adams, U. Bergmann, N. K. Sauter, A. Zouni, J. Messinger, J. Yano and V. K. Yachandra, *Nature*, 2018, **563**, 421-425.
81. M. Suga, F. Akita, K. Yamashita, Y. Nakajima, G. Ueno, H. Li, T. Yamane, K. Hirata, Y. Umena, S. Yonekura, L.-J. Yu, H. Murakami, T. Nomura, T. Kimura, M. Kubo, S. Baba, T. Kumasaka, K. Tono, M. Yabashi, H. Isobe, K. Yamaguchi, M. Yamamoto, H. Ago and J.-R. Shen, *Science*, 2019, **366**, 334.
82. A. Grundmeier and H. Dau, *Biochim. Biophys. Acta Bioenerg.*, 2012, **1817**, 88-105.
83. J. Yano, J. Kern, K.-D. Irrgang, M. J. Latimer, U. Bergmann, P. Glatzel, Y. Pushkar, J. Biesiadka, B. Loll, K. Sauer, J. Messinger, A. Zouni and V. K. Yachandra, *Proc. Natl. Acad. Sci. USA*, 2005, **102**, 12047-12052.
84. M. Grabolle, M. Haumann, C. Müller, P. Liebisch and H. Dau, *J. Biol. Chem.*, 2006, **281**, 4580-4588.
85. A. Galstyan, A. Robertazzi and E. W. Knapp, *J. Am. Chem. Soc.*, 2012, **134**, 7442-7449.
86. P. Chernev, I. Zaharieva, E. Rossini, A. Galstyan, H. Dau and E.-W. Knapp, *J. Phys. Chem. B*, 2016, **120**, 10899-10922.
87. A. Haddy, *Photosynth. Res.*, 2007, **92**, 357-368.
88. A. Haddy, K. V. Lakshmi, G. W. Brudvig and H. A. Frank, *Biophys. J.*, 2004, **87**, 2885-2896.
89. G. C. Dismukes and Y. Siderer, *Proc. Natl. Acad. Sci. U. S. A.*, 1981, **78**, 274-278.
90. J. C. de Paula, W. F. Beck, A.-F. Miller, R. B. Wilson and G. W. Brudvig, *Journal of the Chemical Society, Faraday Transactions* 1987, **83**, 3635-3651.
91. A. Boussac, S. Un, O. Horner and A. W. Rutherford, *Biochemistry*, 1998, **37**, 4001-4007.
92. A. Boussac and A. W. Rutherford, *Biochim. Biophys. Acta Bioenerg.*, 2000, **1457**, 145-156.
93. D. A. Pantazis, W. Ames, N. Cox, W. Lubitz and F. Neese, *Angew. Chem., Int. Ed.*, 2012, **51**, 9935-9940.
94. L. Noodleman, *J. Chem. Phys.*, 1981, **74**, 5737-5743.
95. K. Yamaguchi, *Chem. Phys. Lett.*, 1975, **33**, 330-335.
96. K. Yamaguchi, T. Tsunekawa, Y. Toyoda and T. Fueno, *Chem. Phys. Lett.*, 1988, **143**, 371-376.
97. M. Shoji, K. Koizumi, Y. Kitagawa, T. Kawakami, S. Yamanaka, M. Okumura and K. Yamaguchi, *Chem. Phys. Lett.*, 2006, **432**, 343-347.
98. D. A. Pantazis, M. Orio, T. Petrenko, S. Zein, E. Bill, W. Lubitz, J. Messinger and F. Neese, *Chem. Eur. J.*, 2009, **15**, 5108-5123.
99. D. A. Pantazis, M. Orio, T. Petrenko, S. Zein, W. Lubitz, J. Messinger and F. Neese, *Phys. Chem. Chem. Phys.*, 2009, **11**, 6788-6798.
100. W. Ames, D. A. Pantazis, V. Krewald, N. Cox, J. Messinger, W. Lubitz and F. Neese, *J. Am. Chem. Soc.*, 2011, **133**, 19743-19757.
101. C. Baffert, M. Orio, D. A. Pantazis, C. Duboc, A. G. Blackman, G. Blondin, F. Neese, A. Deronzier and M.-N. Collomb, *Inorg. Chem.*, 2009, **48**, 10281-10288.
102. V. Krewald, F. Neese and D. A. Pantazis, *J. Am. Chem. Soc.*, 2013, **135**, 5726-5739.
103. S. Mukherjee, J. A. Stull, J. Yano, T. C. Stamatatos, K. Pringouri, T. A. Stich, K. A. Abboud, R. D. Britt, V. K. Yachandra and G. Christou, *Proc. Natl. Acad. Sci. U. S. A.*, 2012, **109**, 2257-2262.
104. V. Krewald, M. Retegan, N. Cox, J. Messinger, W. Lubitz, S. DeBeer, F. Neese and D. A. Pantazis, *Chem. Sci.*, 2015, **6**, 1676-1695.
105. T. A. Corry and P. J. O'Malley, *J. Phys. Chem. Lett.*, 2019, **10**, 5226-5230.
106. N. Cox, M. Retegan, F. Neese, D. A. Pantazis, A. Boussac and W. Lubitz, *Science*, 2014, **345**, 804-808.
107. A. Boussac, A. W. Rutherford and M. Sugiura, *Biochim. Biophys. Acta Bioenerg.*, 2015, **1847**, 576-586.
108. G. Zahariou, N. Ioannidis, Y. Sanakis and D. A. Pantazis, *Angew. Chem., Int. Ed.*, 2021, DOI: 10.1002/anie.202012304, DOI: 10.1002/anie.202012304.
109. M. Retegan, V. Krewald, F. Mamedov, F. Neese, W. Lubitz, N. Cox and D. A. Pantazis, *Chem. Sci.*, 2016, **7**, 72-84.
110. D. A. Pantazis, V. Krewald, M. Orio and F. Neese, *Dalton Trans.*, 2010, **39**, 4959-4967.
111. V. Krewald, B. Lassalle-Kaiser, T. T. Boron, C. J. Pollock, J. Kern, M. A. Beckwith, V. K. Yachandra, V. L. Pecoraro, J. Yano, F. Neese and S. DeBeer, *Inorg. Chem.*, 2013, **52**, 12904-12914.
112. C. J. Stein, D. A. Pantazis and V. Krewald, *J. Phys. Chem. Lett.*, 2019, **10**, 6762-6770.

This journal is © The Royal Society of Chemistry 20xx

Please do not adjust margins

Please do not adjust margins

113. T. Lohmiller, V. Krewald, A. Sedoud, A. W. Rutherford, F. Neese, W. Lubitz, D. A. Pantazis and N. Cox, *J. Am. Chem. Soc.*, 2017, **139**, 14412-14424.
114. M. Pérez Navarro, W. M. Ames, H. Nilsson, T. Lohmiller, D. A. Pantazis, L. Rapatskiy, M. M. Nowaczyk, F. Neese, A. Boussac, J. Messinger, W. Lubitz and N. Cox, *Proc. Natl. Acad. Sci. U. S. A.*, 2013, **110**, 15561-15566.
115. T. Lohmiller, V. Krewald, M. Pérez Navarro, M. Retegan, L. Rapatskiy, M. M. Nowaczyk, A. Boussac, F. Neese, W. Lubitz, D. A. Pantazis and N. Cox, *Phys. Chem. Chem. Phys.*, 2014, **16**, 11877-11892.
116. M. Retegan and D. A. Pantazis, *Chem. Sci.*, 2016, **7**, 6463-6476.
117. M. Retegan and D. A. Pantazis, *J. Am. Chem. Soc.*, 2017, **139**, 14340-14343.
118. V. Krewald, F. Neese and D. A. Pantazis, *Isr. J. Chem.*, 2015, **55**, 1219-1232.
119. V. Krewald, M. Retegan, F. Neese, W. Lubitz, D. A. Pantazis and N. Cox, *Inorg. Chem.*, 2016, **55**, 488-501.
120. M. Roemelt and D. A. Pantazis, *Adv. Theory Simul.*, 2019, DOI: 10.1002/adts.201800201, 1800201.
121. V. Krewald and D. A. Pantazis, in *Transition Metals in Coordination Environments: Computational Chemistry and Catalysis Viewpoints*, eds. E. Broclawik, T. Borowski and M. Radoń, Springer International Publishing, Cham, 2019, DOI: 10.1007/978-3-030-11714-6_4, pp. 91-120.
122. M. Roemelt, V. Krewald and D. A. Pantazis, *J. Chem. Theory Comput.*, 2018, **14**, 166-179.
123. D. A. Pantazis, *J. Chem. Theory Comput.*, 2019, **15**, 938-948.
124. T. V. Harris, Y. Kurashige, T. Yanai and K. Morokuma, *J. Chem. Phys.*, 2014, **140**, 054303.
125. S. Sharma, K. Sivalingam, F. Neese and G. K.-L. Chan, *Nat. Chem.*, 2014, **6**, 927-933.
126. M. Spivak, C. Angeli, C. J. Calzado and C. de Graaf, *J. Comput. Chem.*, 2014, **35**, 1665-1671.
127. Y. Kurashige, G. K.-L. Chan and T. Yanai, *Nat. Chem.*, 2013, **5**, 660-666.
128. S. Paul, N. Cox and D. A. Pantazis, *Inorg. Chem.*, 2017, **56**, 3875-3888.
129. M. Munzarová and M. Kaupp, *J. Phys. Chem. A*, 1999, **103**, 9966-9983.
130. M. L. Munzarová, P. Kubáček and M. Kaupp, *J. Am. Chem. Soc.*, 2000, **122**, 11900-11913.
131. S. Schinzel, J. Schraut, A. V. Arbuznikov, P. E. M. Siegbahn and M. Kaupp, *Chem. Eur. J.*, 2010, **16**, 10424-10438.
132. J. Schraut, A. V. Arbuznikov, S. Schinzel and M. Kaupp, *ChemPhysChem*, 2011, **12**, 3170-3179.
133. M. Orio, D. A. Pantazis, T. Petrenko and F. Neese, *Inorg. Chem.*, 2009, **48**, 7251-7260.
134. C. J. Schattenberg, T. M. Maier and M. Kaupp, *J. Chem. Theory Comput.*, 2018, **14**, 5653-5672.
135. A. Wodyński and M. Kaupp, *J. Chem. Theory Comput.*, 2020, **16**, 314-325.
136. M. Saitow and F. Neese, *J. Chem. Phys.*, 2018, **149**, 034104.
137. R. J. Gómez-Piñeiro, D. A. Pantazis and M. Orio, *ChemPhysChem*, 2020, **21**, 2667-2679.
138. G. Blondin, R. Davydov, C. Philouze, M.-F. Charlot, S. Styring, B. Åkermark, J.-J. Girerd and A. Boussac, *J. Chem. Soc., Dalton Trans.*, 1997, DOI: 10.1039/A703381H 4069-4074.
139. J. Yano, J. Kern, K. Sauer, M. J. Latimer, Y. Pushkar, J. Biesiadka, B. Loll, W. Saenger, J. Messinger, A. Zouni and V. K. Yachandra, *Science*, 2006, **314**, 821-825.
140. E. M. Sproviero, J. A. Gascon, J. P. McEvoy, G. W. Brudvig and V. S. Batista, *Coord. Chem. Rev.*, 2008, **252**, 395-415.
141. P. E. M. Siegbahn, *Inorg. Chem.*, 2008, **47**, 1779-1786.
142. E. M. Sproviero, J. A. Gascon, J. P. McEvoy, G. W. Brudvig and V. S. Batista, *J. Am. Chem. Soc.*, 2008, **130**, 6728-6730.
143. P. E. M. Siegbahn, *Acc. Chem. Res.*, 2009, **42**, 1871-1880.
144. J. M. Peloquin, K. A. Campbell and R. D. Britt, *J. Am. Chem. Soc.*, 1998, **120**, 6840-6841.
145. J. M. Peloquin, K. A. Campbell, D. W. Randall, M. A. Evanchik, V. L. Pecoraro, W. H. Armstrong and R. D. Britt, *J. Am. Chem. Soc.*, 2000, **122**, 10926-10942.
146. R. D. Britt, K. A. Campbell, J. M. Peloquin, M. L. Gilchrist, C. P. Aznar, M. M. Dicus, J. Robblee and J. Messinger, *Biochim. Biophys. Acta*, 2004, **1655**, 158-171.
147. L. V. Kulik, B. Epel, W. Lubitz and J. Messinger, *J. Am. Chem. Soc.*, 2005, **127**, 2392-2393.
148. L. V. Kulik, B. Epel, W. Lubitz and J. Messinger, *J. Am. Chem. Soc.*, 2007, **129**, 13421-13435.
149. N. Cox, L. Rapatskiy, J.-H. Su, D. A. Pantazis, M. Sugiura, L. Kulik, P. Dorlet, A. W. Rutherford, F. Neese, A. Boussac, W. Lubitz and J. Messinger, *J. Am. Chem. Soc.*, 2011, **133**, 3635-3648.
150. N. Cox, D. A. Pantazis, F. Neese and W. Lubitz, *Acc. Chem. Res.*, 2013, **46**, 1588-1596.
151. C. Mehlich and C. van Wüllen, *J. Phys. Chem. C*, 2018, **123**, 7717-7730.
152. C. Mehlich and C. van Wüllen, *Phys. Chem. Chem. Phys.*, 2019, **21**, 22902-22909.
153. N. J. Beal, T. A. Corry and P. J. O'Malley, *J. Phys. Chem. B*, 2017, **121**, 11273-11283.
154. N. J. Beal, T. A. Corry and P. J. O'Malley, *J. Phys. Chem. B*, 2018, **122**, 1394-1407.
155. J. Messinger, J. H. Robblee, U. Bergmann, C. Fernandez, P. Glatzel, H. Visser, R. M. Cinco, K. L. McFarlane, E. Bellacchio, S. A. Pizarro, S. P. Cramer, K. Sauer, M. P. Klein and V. K. Yachandra, *J. Am. Chem. Soc.*, 2001, **123**, 7804-7820.
156. H. Dau, P. Liebisch and M. Haumann, *Phys. Scr.*, 2005, **2005**, 844.
157. H. Dau and M. Haumann, *Biochim. Biophys. Acta Bioenerg.*, 2007, **1767**, 472-483.
158. A. Boussac, *Biochim. Biophys. Acta Bioenerg.*, 2019, **1860**, 508-518.
159. D. A. Marchiori, R. J. Debus and R. D. Britt, *Biochemistry*, 2020, **59**, 4864-4872.
160. M. Chrysina, E. Heyno, Y. Kutin, M. Reus, H. Nilsson, M. M. Nowaczyk, S. DeBeer, F. Neese, J. Messinger, W. Lubitz and N. Cox, *Proc. Natl. Acad. Sci. U. S. A.*, 2019, **116**, 16841.
161. D. A. Pantazis, *Inorganics*, 2019, **7**, 55.
162. T. A. Corry and P. J. O'Malley, *J. Phys. Chem. Lett.*, 2018, **9**, 6269-6274.
163. H. Isobe, M. Shoji, T. Suzuki, J.-R. Shen and K. Yamaguchi, *J. Chem. Theory Comput.*, 2019, **15**, 2375-2391.
164. Y. Pushkar, K. M. Davis and M. C. Palenik, *J. Phys. Chem. Lett.*, 2018, **9**, 3525-3531.
165. P. H. Oyala, T. A. Stich and R. D. Britt, *Photosynth. Res.*, 2015, **124**, 7-18.
166. L. Rapatskiy, N. Cox, A. Savitsky, W. M. Ames, J. Sander, M. M. Nowaczyk, M. Rögner, A. Boussac, F. Neese, J. Messinger and W. Lubitz, *J. Am. Chem. Soc.*, 2012, **134**, 16619-16634.
167. P. H. Oyala, T. A. Stich, J. A. Stull, F. Yu, V. L. Pecoraro and R. D. Britt, *Biochemistry*, 2014, **53**, 7914-7928.
168. P. H. Oyala, T. A. Stich, R. J. Debus and R. D. Britt, *J. Am. Chem. Soc.*, 2015, **137**, 8829-8837.
169. D. A. Marchiori, P. H. Oyala, R. J. Debus, T. A. Stich and R. D. Britt, *J. Phys. Chem. B*, 2018, **122**, 1588-1599.
170. J. Schraut and M. Kaupp, *Chem. Eur. J.*, 2014, **20**, 7300-7308.
171. Y. Guo, L.-L. He, D.-X. Zhao, L.-D. Gong, C. Liu and Z.-Z. Yang, *Phys. Chem. Chem. Phys.*, 2016, **18**, 31551-31565.
172. A. Boussac, Y. Deligiannakis and A. W. Rutherford, in *Photosynthesis: Mechanisms and Effects, Vol. II*, ed. G. Garab, Kluwer Academic Publishers, Dordrecht, 1998, pp. 1233-1240.
173. Z. Deák, S. Peterson, P. Geijer, K. A. Åhrling and S. Styring, *Biochim. Biophys. Acta Bioenerg.*, 1999, **1412**, 240-249.
174. K. A. Åhrling, M. C. W. Evans, J. H. A. Nugent and R. J. Pace, *Biochim. Biophys. Acta Bioenerg.*, 2004, **1656**, 66-77.
175. J.-H. Su, K. G. V. Havelius, F. Mamedov, F. M. Ho and S. Styring, *Biochemistry*, 2006, **45**, 7617-7627.
176. F. M. Ho and S. Styring, *Biochim. Biophys. Acta Bioenerg.*, 2008, **1777**, 140-153.
177. B. Nöring, D. Shevela, G. Renger and J. Messinger, *Photosynth. Res.*, 2008, **98**, 251-260.
178. J.-H. Su, N. Cox, W. Ames, D. A. Pantazis, L. Rapatskiy, T. Lohmiller, L. V. Kulik, P. Dorlet, A. W. Rutherford, F. Neese, A.

Please do not adjust margins

Please do not adjust margins

Boussac, W. Lubitz and J. Messinger, *Biochim. Biophys. Acta Bioenerg.*, 2011, **1807**, 829-840.
179. M. Askerka, D. J. Vinyard, G. W. Brudvig and V. S. Batista, *Biochemistry*, 2015, **54**, 5783-5786.
180. M. Retegan, N. Cox, D. A. Pantazis and F. Neese, *Inorg. Chem.*, 2014, **53**, 11785-11793.
181. H. Mino and H. Nagashima, *J. Phys. Chem. B*, 2019, **124**, 128-133.
182. M. Retegan, N. Cox, W. Lubitz, F. Neese and D. A. Pantazis, *Phys. Chem. Chem. Phys.*, 2014, **16**, 11901-11910.
183. A. Sirohiwal, F. Neese and D. A. Pantazis, *J. Am. Chem. Soc.*, 2019, **141**, 3217-3231.
184. P. E. M. Siegbahn, *J. Am. Chem. Soc.*, 2013, **135**, 9442-9449.
185. P. E. M. Siegbahn, *Biochim. Biophys. Acta Bioenerg.*, 2013, **1827**, 1003-1019.
186. D. Bovi, D. Narzi and L. Guidoni, *Angew. Chem., Int. Ed.*, 2013, **52**, 11744-11749.
187. M. Chrysina, J. C. de Mendonça Silva, G. Zahariou, D. A. Pantazis and N. Ioannidis, *J. Phys. Chem. B*, 2019, **123**, 3068-3078.
188. H. Sakamoto, T. Shimizu, R. Nagao and T. Noguchi, *J. Am. Chem. Soc.*, 2017, **139**, 2022-2029.
189. K. Kawashima, K. Saito and H. Ishikita, *Biochemistry*, 2018, **57**, 4997-5004.
190. V. Krewald, F. Neese and D. A. Pantazis, *Phys. Chem. Chem. Phys.*, 2016, **18**, 10739-10750.
191. E. Y. Tsui and T. Agapie, *Proc. Natl. Acad. Sci. U. S. A.*, 2013, **110**, 10084-10088.
192. E. Y. Tsui, R. Tran, J. Yano and T. Agapie, *Nat. Chem.*, 2013, **5**, 293-299.
193. M. Retegan, F. Neese and D. A. Pantazis, *J. Chem. Theory Comput.*, 2013, **9**, 3832-3842.
194. M. Shoji, H. Isobe, S. Yamanaka, Y. Umena, K. Kawakami, N. Kamiya, J.-R. Shen, T. Nakajima and K. Yamaguchi, *Mol. Phys.*, 2015, **113**, 359-384.
195. M. Askerka, G. W. Brudvig and V. S. Batista, *Acc. Chem. Res.*, 2017, **50**, 41-48.
196. S. Nakamura, M. Capone, D. Narzi and L. Guidoni, *Phys. Chem. Chem. Phys.*, 2019, DOI: 10.1039/C9CP04605D.
197. D. Narzi, D. Bovi and L. Guidoni, *Proc. Natl. Acad. Sci. U. S. A.*, 2014, **111**, 8723-8728.
198. M. Shoji, H. Isobe, Y. Shigeta, T. Nakajima and K. Yamaguchi, *Chem. Phys. Lett.*, 2018, **698**, 138-146.
199. D. A. Pantazis, *Chem. Phys. Lett.*, 2020, **753**, 137629.
200. N. Cox, D. A. Pantazis and W. Lubitz, *Annu. Rev. Biochem.*, 2020, **89**, 795-820.
201. J.-R. Shen, *Annu. Rev. Plant Biol.*, 2015, **66**, 23-48.
202. K. Yamaguchi, M. Shoji, H. Isobe, S. Yamanaka, T. Kawakami, S. Yamada, M. Katouda and T. Nakajima, *Mol. Phys.*, 2018, **116**, 717-745.
203. G. Zahariou and N. Ioannidis, *Photosynth. Res.*, 2016, **130**, 417-426.
204. H. Nilsson, F. Rappaport, A. Boussac and J. Messinger, *Nat. Commun.*, 2014, **5**, 4305.
205. M. Haumann, P. Liebisch, C. Müller, M. Barra, M. Grabolle and H. Dau, *Science*, 2005, **310**, 1019-1021.
206. V. Krewald, F. Neese and D. A. Pantazis, *J. Inorg. Biochem.*, 2019, **199**, 110797.
207. P. E. M. Siegbahn, *Chem. Eur. J.*, 2008, **14**, 8290-8302.
208. X. Li and P. E. M. Siegbahn, *Phys. Chem. Chem. Phys.*, 2015, **17**, 12168-12174.
209. Y. Guo, H. Li, L.-L. He, D.-X. Zhao, L.-D. Gong and Z.-Z. Yang, *Phys. Chem. Chem. Phys.*, 2017, **19**, 13909-13923.
210. M. Ibrahim, T. Fransson, R. Chatterjee, M. H. Cheah, R. Hussein, L. Lassalle, K. D. Sutherlin, I. D. Young, F. D. Fuller, S. Gul, I.-S. Kim, P. S. Simon, C. de Lichtenberg, P. Chernev, I. Bogacz, C. C. Pham, A. M. Orville, N. Saichek, T. Northen, A. Batyuk, S. Carbajo, R. Alonso-Mori, K. Tono, S. Owada, A. Bhowmick, R. Bolotovsky, D. Mendez, N. W. Moriarty, J. M. Holton, H. Dobbek, A. S. Brewster, P. D. Adams, N. K. Sauter, U. Bergmann, A. Zouni, J. Messinger, J. Kern, V. K. Yachandra and J. Yano, *Proc. Natl. Acad. Sci. U. S. A.*, 2020, **117**, 12624-12635.
211. H. Isobe, M. Shoji, J.-R. Shen and K. Yamaguchi, *Inorg. Chem.*, 2016, **55**, 502-511.
212. Y. Pushkar, A. K. Ravari, S. C. Jensen and M. Palenik, *J. Phys. Chem. Lett.*, 2019, **10**, 5284-5291.
213. D. Narzi, M. Capone, D. Bovi and L. Guidoni, *Chem. Eur. J.*, 2018, **24**, 10820-10828.
214. M. Swart and M. Costas, *Spin States in Biochemistry and Inorganic Chemistry*, John Wiley & Sons, Chichester, 2016.
215. C. Riplinger and F. Neese, *J. Chem. Phys.*, 2013, **138**, 034106.
216. M. Saitow, U. Becker, C. Riplinger, E. F. Valeev and F. Neese, *J. Chem. Phys.*, 2017, **146**, 164105.
217. Y. Guo, C. Riplinger, U. Becker, D. G. Liakos, Y. Minenkov, L. Cavallo and F. Neese, *J. Chem. Phys.*, 2018, **148**, 011101.
218. P. Paiva, M. J. Ramos and P. A. Fernandes, *J. Comput. Chem.*, 2020, **41**, 2459-2468.
219. D. G. Liakos, Y. Guo and F. Neese, *J. Phys. Chem. A*, 2019, **124**, 90-100.
220. S. E. Neale, D. A. Pantazis and S. A. Macgregor, *Dalton Trans.*, 2020, **49**, 6478-6487.
221. B. M. Flöser, Y. Guo, C. Riplinger, F. Tuczek and F. Neese, *J. Chem. Theory Comput.*, 2020, **16**, 2224-2235.
222. K. A. Vincent, A. Parkin and F. A. Armstrong, *Chem. Rev.*, 2007, **107**, 4366-4413.
223. A. L. De Lacey, V. M. Fernández, M. Rousset and R. Cammack, *Chem. Rev.*, 2007, **107**, 4304-4330.
224. P. E. M. Siegbahn, J. W. Tye and M. B. Hall, *Chem. Rev.*, 2007, **107**, 4414-4435.
225. A. Volbeda, M.-H. Charon, C. Piras, E. C. Hatchikian, M. Frey and J. C. Fontecilla-Camps, *Nature*, 1995, **373**, 580-587.
226. V. Vaissier and T. Van Voorhis, *Essays Biochem.*, 2017, **61**, 293-303.
227. F. Wittkamp, M. Senger, S. T. Stripp and U. P. Apfel, *Chem. Commun.*, 2018, **54**, 5934-5942.
228. H. Land, M. Senger, G. Berggren and S. T. Stripp, *ACS Catal.*, 2020, **10**, 7069-7086.
229. B. H. Solis and S. Hammes-Schiffer, *Inorg. Chem.*, 2014, **53**, 6427-6443.
230. S. Hammes-Schiffer, *Acc. Chem. Res.*, 2018, **51**, 1975-1983.
231. S. Hammes-Schiffer, *Acc. Chem. Res.*, 2017, **50**, 561-566.
232. A. Petrenko and M. Stein, in *Spin States in Biochemistry and Inorganic Chemistry*, 2015, DOI: https://doi.org/10.1002/9781118898277.ch14, pp. 327-367.
233. G. Dong, Q. M. Phung, K. Pierloot and U. Ryde, *Inorg. Chem.*, 2018, **57**, 15289-15298.
234. G. Dong and U. Ryde, *J. Biol. Inorg. Chem.*, 2016, **21**, 383-394.
235. A. R. Finkelmann, M. T. Stiebritz and M. Reiher, *Chem. Commun.*, 2013, **49**, 8099-8101.
236. E. D. Hedegård, J. Kongsted and U. Ryde, *Angew. Chem., Int. Ed.*, 2015, **54**, 6246-6250.
237. C. Greco, M. Bruschi, P. Fantucci, U. Ryde and L. De Gioia, *J. Am. Chem. Soc.*, 2011, **133**, 18742-18749.
238. U. Ryde, C. Greco and L. De Gioia, *J. Am. Chem. Soc.*, 2010, **132**, 4512-4513.
239. B. Ginovska, S. Raugei and W. J. Shaw, *Methods Enzymol.*, 2016, **578**, 73-101.
240. O. Sode and G. A. Voth, *J. Chem. Phys.*, 2014, **141**, 22D527.
241. V. H. Teixeira, C. M. Soares and A. M. Baptista, *Proteins: Struct., Funct., Bioinf.*, 2008, **70**, 1010-1022.
242. M. McCullagh and G. A. Voth, *J. Phys. Chem. B*, 2013, **117**, 4062-4071.
243. S. Qiu, L. M. Azofra, D. R. MacFarlane and C. Sun, *Phys. Chem. Chem. Phys.*, 2016, **18**, 15369-15374.
244. C. H. Chang, *J. Phys. Chem. A*, 2011, **115**, 8691-8704.
245. M. Z. Makoś, M. Freindorf, D. Sethio and E. Kraka, *Theor. Chem. Acc.*, 2019, **138**, 76.
246. P. Jayapal, D. Robinson, M. Sundararajan, I. H. Hillier and J. J. W. McDouall, *Phys. Chem. Chem. Phys.*, 2008, **10**, 1734-1738.
247. M. G. Delcey, K. Pierloot, Q. M. Phung, S. Vancoillie, R. Lindh and U. Ryde, *Phys. Chem. Chem. Phys.*, 2014, **16**, 7927-7938.
248. G. Dong, Q. M. Phung, S. D. Hallaert, K. Pierloot and U. Ryde, *Phys. Chem. Chem. Phys.*, 2017, **19**, 10590-10601.

This journal is © The Royal Society of Chemistry 20xx

Please do not adjust margins

Please do not adjust margins

249. G. Dong, U. Ryde, H. J. Aa Jensen and E. D. Hedegard, *Phys. Chem. Chem. Phys.*, 2018, **20**, 794-801.
250. C. Greco, P. Fantucci, U. Ryde and L. d. Gioia, *Int. J. Quantum Chem.*, 2011, **111**, 3949-3960.
251. C. Greco, A. Silakov, M. Bruschi, U. Ryde, L. De Gioia and W. Lubitz, *Eur. J. Inorg. Chem.*, 2011, **2011**, 1043-1049.
252. L. Bertini, M. Bruschi, U. Cosentino, C. Greco, G. Moro, G. Zampella and L. De Gioia, in *Metalloproteins: Methods and Protocols*, eds. J. C. Fontecilla-Camps and Y. Nicolet, Humana Press, Totowa, NJ, 2014, DOI: 10.1007/978-1-62703-794-5_14, pp. 207-268.
253. J.-M. Mouesca, J. C. Fontecilla-Camps and P. Amara, *Angew. Chem., Int. Ed.*, 2013, **52**, 2002-2006.
254. M.-E. Pandelia, D. Bykov, R. Izsak, P. Infossi, M.-T. Giudici-Orticoni, E. Bill, F. Neese and W. Lubitz, *Proc. Natl. Acad. Sci. U. S. A.*, 2013, **110**, 483-488.
255. V. Pelmenschikov and M. Kaupp, *J. Am. Chem. Soc.*, 2013, **135**, 11809-11823.
256. L. Yu, C. Greco, M. Bruschi, U. Ryde, L. De Gioia and M. Reiher, *Inorg. Chem.*, 2011, **50**, 3888-3900.
257. D. W. Mulder, M. W. Ratzloff, M. Bruschi, C. Greco, E. Koonce, J. W. Peters and P. W. King, *J. Am. Chem. Soc.*, 2014, **136**, 15394-15402.
258. P. S. Corrigan, J. L. Tirsch and A. Silakov, *J. Am. Chem. Soc.*, 2020, **142**, 12409-12419.
259. S. Mebs, M. Senger, J. Duan, F. Wittkamp, U.-P. Apfel, T. Happe, M. Winkler, S. T. Stripp and M. Haumann, *J. Am. Chem. Soc.*, 2017, **139**, 12157-12160.
260. C. C. Pham, D. W. Mulder, V. Pelmenschikov, P. W. King, M. W. Ratzloff, H. Wang, N. Mishra, E. E. Alp, J. Zhao, M. Y. Hu, K. Tamasaku, Y. Yoda and S. P. Cramer, *Angew. Chem., Int. Ed.*, 2018, **57**, 10605-10609.
261. T. Krämer, M. Kampa, W. Lubitz, M. van Gastel and F. Neese, *ChemBioChem*, 2013, **14**, 1898-1905.
262. M. Kampa, W. Lubitz, M. van Gastel and F. Neese, *J. Biol. Inorg. Chem.*, 2012, **17**, 1269-1281.
263. J. A. Birrell, V. Pelmenschikov, N. Mishra, H. Wang, Y. Yoda, K. Tamasaku, T. B. Rauchfuss, S. P. Cramer, W. Lubitz and S. DeBeer, *J. Am. Chem. Soc.*, 2020, **142**, 222-232.
264. V. Pelmenschikov, J. A. Birrell, C. C. Pham, N. Mishra, H. Wang, C. Sommer, E. Reijerse, C. P. Richers, K. Tamasaku, Y. Yoda, T. B. Rauchfuss, W. Lubitz and S. P. Cramer, *J. Am. Chem. Soc.*, 2017, **139**, 16894-16902.
265. E. J. Reijerse, C. C. Pham, V. Pelmenschikov, R. Gilbert-Wilson, A. Adamska-Venkatesh, J. F. Siebel, L. B. Gee, Y. Yoda, K. Tamasaku, W. Lubitz, T. B. Rauchfuss and S. P. Cramer, *J. Am. Chem. Soc.*, 2017, **139**, 4306-4309.
266. S. Kamali, H. Wang, D. Mitra, H. Ogata, W. Lubitz, B. C. Manor, T. B. Rauchfuss, D. Byrne, V. Bonnefoy, F. E. Jenney Jr., M. W. W. Adams, Y. Yoda, E. Alp, J. Zhao and S. P. Cramer, *Angew. Chem., Int. Ed.*, 2013, **52**, 724-728.
267. L. Lauterbach, H. Wang, M. Horch, L. B. Gee, Y. Yoda, Y. Tanaka, I. Zebger, O. Lenz and S. P. Cramer, *Chem. Sci.*, 2015, **6**, 1055-1060.
268. H. Ogata, T. Krämer, H. Wang, D. Schilter, V. Pelmenschikov, M. van Gastel, F. Neese, T. B. Rauchfuss, L. B. Gee, A. D. Scott, Y. Yoda, Y. Tanaka, W. Lubitz and S. P. Cramer, *Nat. Commun.*, 2015, **6**, 7890.
269. M. Kampa, M.-E. Pandelia, W. Lubitz, M. van Gastel and F. Neese, *J. Am. Chem. Soc.*, 2013, **135**, 3915-3925.
270. G. Berggren, A. Adamska, C. Lambertz, T. R. Simmons, J. Esselborn, M. Atta, S. Gambarelli, J. M. Mouesca, E. Reijerse, W. Lubitz, T. Happe, V. Artero and M. Fontecave, *Nature*, 2013, **499**, 66-69.
271. E. J. Reijerse, V. Pelmenschikov, J. A. Birrell, C. P. Richers, M. Kaupp, T. B. Rauchfuss, S. P. Cramer and W. Lubitz, *J. Phys. Chem. Lett.*, 2019, **10**, 6794-6799.
272. E. Reijerse, J. A. Birrell and W. Lubitz, *J. Phys. Chem. Lett.*, 2020, **11**, 4597-4602.
273. S. G. Tabrizi, V. Pelmenschikov, L. Noodleman and M. Kaupp, *J. Chem. Theory Comput.*, 2016, **12**, 174-187.
274. E. D. Hedegård, S. Knecht, U. Ryde, J. Kongsted and T. Saue, *Phys. Chem. Chem. Phys.*, 2014, **16**, 4853-4863.
275. J. Gubler, A. R. Finkelmann and M. Reiher, *Inorg. Chem.*, 2013, **52**, 14205-14215.
276. S. Ogo, T. Kishima, T. Yatabe, K. Miyazawa, R. Yamasaki, T. Matsumoto, T. Ando, M. Kikkawa, M. Isegawa, K.-S. Yoon and S. Hayami, *Science Advances*, 2020, **6**, eaaz8181.
277. F. Neese, F. Wennmohs, U. Becker and C. Riplinger, *J. Chem. Phys.*, 2020, **152**, 224108.
278. F. Aquilante, J. Autschbach, A. Baiardi, S. Battaglia, V. A. Borin, L. F. Chibotaru, I. Conti, L. D. Vico, M. Delcey, I. F. Galván, N. Ferré, L. Freitag, M. Garavelli, X. Gong, S. Knecht, E. D. Larsson, R. Lindh, M. Lundberg, P. Å. Malmqvist, A. Nenov, J. Norell, M. Odelius, M. Olivucci, T. B. Pedersen, L. Pedraza-González, Q. M. Phung, K. Pierloot, M. Reiher, I. Schapiro, J. Segarra-Martí, F. Segatta, L. Seijo, S. Sen, D.-C. Sergentu, C. J. Stein, L. Ungur, M. Vacher, A. Valentini and V. Veryazov, *J. Chem. Phys.*, 2020, **152**, 214117.
279. S. G. Balasubramani, G. P. Chen, S. Coriani, M. Diedenhofen, M. S. Frank, Y. J. Franzke, F. Furche, R. Grotjahn, M. E. Harding, C. Hättig, A. Hellweg, B. Helmich-Paris, C. Holzer, U. Huniar, M. Kaupp, A. M. Khah, S. K. Khani, T. Müller, F. Mack, B. D. Nguyen, S. M. Parker, E. Perlt, D. Rappoport, K. Reiter, S. Roy, M. Rückert, G. Schmitz, M. Sierka, E. Tapavicza, D. P. Tew, C. v. Wüllen, V. K. Voora, F. Weigend, A. Wodyński and J. M. Yu, *J. Chem. Phys.*, 2020, **152**, 184107.
280. E. Aprà, E. J. Bylaska, W. A. d. Jong, N. Govind, K. Kowalski, T. P. Straatsma, M. Valiev, H. J. J. v. Dam, Y. Alexeev, J. Anchell, V. Anisimov, F. W. Aquino, R. Atta-Fynn, J. Autschbach, N. P. Bauman, J. C. Becca, D. E. Bernholdt, K. Bhaskaran-Nair, S. Bogatko, P. Borowski, J. Boschen, J. Brabec, A. Bruner, E. Cauët, Y. Chen, G. N. Chuev, C. J. Cramer, J. Daily, M. J. O. Deegan, T. H. DunningJr., M. Dupuis, K. G. Dyall, G. I. Fann, S. A. Fischer, A. Fonari, H. Früchtl, L. Gagliardi, J. Garza, N. Gawande, S. Ghosh, K. Glaesemann, A. W. Götz, J. Hammond, V. Helms, E. D. Hermes, K. Hirao, S. Hirata, M. Jacquelin, L. Jensen, B. G. Johnson, H. Jónsson, R. A. Kendall, M. Klemm, R. Kobayashi, V. Konkov, S. Krishnamoorthy, M. Krishnan, Z. Lin, R. D. Lins, R. J. Littlefield, A. J. Logsdail, K. Lopata, W. Ma, A. V. Marenich, J. M. d. Campo, D. Mejia-Rodriguez, J. E. Moore, J. M. Mullin, T. Nakajima, D. R. Nascimento, J. A. Nichols, P. J. Nichols, J. Nieplocha, A. Otero-de-la-Roza, B. Palmer, A. Panyala, T. Pirojsirikul, B. Peng, R. Peverati, J. Pittner, L. Pollack, R. M. Richard, P. Sadayappan, G. C. Schatz, W. A. Shelton, D. W. Silverstein, D. M. A. Smith, T. A. Soares, D. Song, M. Swart, H. L. Taylor, G. S. Thomas, V. Tipparaju, D. G. Truhlar, K. Tsemekhman, T. V. Voorhis, Á. Vázquez-Mayagoitia, P. Verma, O. Villa, A. Vishnu, K. D. Vogiatzis, D. Wang, J. H. Weare, M. J. Williamson, T. L. Windus, K. Woliński, A. T. Wong, Q. Wu, C. Yang, Q. Yu, M. Zacharias, Z. Zhang, Y. Zhao and R. J. Harrison, *J. Chem. Phys.*, 2020, **152**, 184102.
281. H. Tang and M. B. Hall, *J. Am. Chem. Soc.*, 2017, **139**, 18065-18070.
282. D. Brazzolotto, L. Wang, H. Tang, M. Gennari, N. Queyriaux, C. Philouze, S. Demeshko, F. Meyer, M. Orio, V. Artero, M. B. Hall and C. Duboc, *ACS Catal.*, 2018, **8**, 10658-10667.
283. J. L. Barilone, H. Ogata, W. Lubitz and M. van Gastel, *Phys. Chem. Chem. Phys.*, 2015, **17**, 16204-16212.
284. C. V. Popescu, S. Ding, P. Ghosh, M. B. Hall and M. Cohara, *Inorg. Chem.*, 2019, **58**, 7069-7077.
285. S. Niu, A. E. Nelson, P. De La Torre, H. Li, C. F. Works and M. B. Hall, *Inorg. Chem.*, 2019, **58**, 13737-13741.
286. A. Kochem, E. Bill, F. Neese and M. van Gastel, *Chem. Commun.*, 2015, **51**, 2099-2102.
287. M. T. Huynh, W. Wang, T. B. Rauchfuss and S. Hammes-Schiffer, *Inorg. Chem.*, 2014, **53**, 10301-10311.
288. G. M. Chambers, M. T. Huynh, Y. Li, S. Hammes-Schiffer, T. B. Rauchfuss, E. Reijerse and W. Lubitz, *Inorg. Chem.*, 2016, **55**, 419-431.
289. A. Kochem, T. Weyhermüller, F. Neese and M. van Gastel, *Organometallics*, 2015, **34**, 995-1000.

Please do not adjust margins

Please do not adjust margins

290. A. Kochem, F. Neese and M. van Gastel, *J. Phys. Chem. C*, 2014, **118**, 2350-2360.
291. A. Barrozo and M. Orio, *ChemSusChem*, 2019, **12**, 4905-4915.
292. B. H. Solis and S. Hammes-Schiffer, *J. Am. Chem. Soc.*, 2011, **133**, 19036-19039.
293. A. Bhattacharjee, E. S. Andreiadis, M. Chavarot-Kerlidou, M. Fontecave, M. J. Field and V. Artero, *Chemistry*, 2013, **19**, 15166-15174.
294. B. H. Solis and S. Hammes-Schiffer, *Inorg. Chem.*, 2011, **50**, 11252-11262.
295. Y. A. Small, D. L. DuBois, E. Fujita and J. T. Muckerman, *Energy Environ. Sci.*, 2011, **4**.
296. S. Horvath, L. E. Fernandez, A. M. Appel and S. Hammes-Schiffer, *Inorg. Chem.*, 2013, **52**, 3643-3652.
297. M. Rakowski DuBois and D. L. DuBois, *Chem. Soc. Rev.*, 2009, **38**, 62-72.
298. W. J. Shaw, M. L. Helm and D. L. DuBois, *Biochim. Biophys. Acta Bioenerg.*, 2013, **1827**, 1123-1139.
299. C. Pieri, A. Bhattacharjee, A. Barrozo, B. Faure, M. Giorgi, J. Fize, M. Réglier, M. Field, M. Orio, V. Artero and R. Hardré, *Chem. Commun.*, 2020, **56**, 11106-11109.
300. J. T. Muckerman and E. Fujita, *Chem. Commun.*, 2011, **47**, 12456-12458.
301. R. Jain, A. A. Mamun, R. M. Buchanan, P. M. Kozlowski and C. A. Grapperhaus, *Inorg. Chem.*, 2018, **57**, 13486-13493.
302. A. Z. Haddad, B. D. Garabato, P. M. Kozlowski, R. M. Buchanan and C. A. Grapperhaus, *J. Am. Chem. Soc.*, 2016, **138**, 7844-7847.
303. H. Tang, E. N. Brothers, C. A. Grapperhaus and M. B. Hall, *ACS Catal.*, 2020, **10**, 3778-3789.
304. B. H. Solis, A. G. Maher, D. K. Dogutan, D. G. Nocera and S. Hammes-Schiffer, *Proc. Natl. Acad. Sci. U. S. A.*, 2016, **113**, 485-492.
305. R.-Z. Liao, M. Wang, L. Sun and P. E. M. Siegbahn, *Dalton Trans.*, 2015, **44**, 9736-9739.
306. K. Ye, Y.-Y. Li and R.-Z. Liao, *RSC Adv.*, 2016, **6**, 90035-90045.
307. M. Papadakis, A. Barrozo, T. Straistari, N. Queyriaux, A. Putri, J. Fize, M. Giorgi, M. Réglier, J. Massin, R. Hardré and M. Orio, *Dalton Trans.*, 2020, **49**, 5064-5073.
308. T. Straistari, R. Hardré, J. Massin, M. Attolini, B. Faure, M. Giorgi, M. Réglier and M. Orio, *Eur. J. Inorg. Chem.*, 2018, **2018**, 2259-2266.
309. A. Barrozo and M. Orio, *RSC Adv.*, 2021, **11**, 5232-5238.
310. G. M. Chambers, J. Mitra, T. B. Rauchfuss and M. Stein, *Inorg. Chem.*, 2014, **53**, 4243-4249.
311. L. Vaccaro, V. Artero, S. Canaguier, M. Fontecave and M. J. Field, *Dalton Trans.*, 2010, **39**, 3043-3049.
312. R. Das, F. Neese and M. van Gastel, *Phys. Chem. Chem. Phys.*, 2016, **18**, 24681-24692.
313. S. Kaur-Ghumaan and M. Stein, *Dalton Trans.*, 2014, **43**, 9392-9405.
314. M. T. Huynh, D. Schilter, S. Hammes-Schiffer and T. B. Rauchfuss, *J. Am. Chem. Soc.*, 2014, **136**, 12385-12395.
315. D. Schilter, M. J. Nilges, M. Chakrabarti, P. A. Lindahl, T. B. Rauchfuss and M. Stein, *Inorg. Chem.*, 2012, **51**, 2338-2348.
316. J. M. Keith and M. B. Hall, *Inorg. Chem.*, 2010, **49**, 6378-6380.
317. M. Panneerselvam and M. Jaccob, *Inorg. Chem.*, 2018, **57**, 8116-8127.
318. B. H. Solis, Y. Yu and S. Hammes-Schiffer, *Inorg. Chem.*, 2013, **52**, 6994-6999.
319. S. Horvath, L. E. Fernandez, A. V. Soudackov and S. Hammes-Schiffer, *Proc. Natl. Acad. Sci. U. S. A.*, 2012, **109**, 15663-15668.
320. L. E. Fernandez, S. Horvath and S. Hammes-Schiffer, *J. Phys. Chem. Lett.*, 2013, **4**, 542-546.
321. J. P. Layfield and S. Hammes-Schiffer, *Chem. Rev.*, 2014, **114**, 3466-3494.
322. D. M. A. Smith, Y. Xiong, T. P. Straatsma, K. M. Rosso and T. C. Squier, *J. Chem. Theory Comput.*, 2012, **8**, 2103-2114.
323. P.-h. Wang, R. B. Best and J. Blumberger, *J. Am. Chem. Soc.*, 2011, **133**, 3548-3556.
324. P. H. Wang, D. De Sancho, R. B. Best and J. Blumberger, in *Methods Enzymol.*, ed. G. A. Voth, Academic Press, 2016, vol. 578, pp. 299-326.
325. L. Bertini, M. Bruschi, L. d. Gioia, P. Fantucci, C. Greco and G. Zampella, *Top. Curr. Chem.*, 2007, **268**, 1-46.
326. S. Qiu, Q. Li, Y. Xu, S. Shen and C. Sun, *WIREs Computational Molecular Science*, 2020, **10**, e1422.
327. S. Qiu, L. M. Azofra, D. R. MacFarlane and C. Sun, *ACS Catal.*, 2016, **6**, 5541-5548.
328. S. Qiu, L. M. Azofra, D. R. MacFarlane and C. Sun, *Phys. Chem. Chem. Phys.*, 2018, **20**, 6735-6743.
329. P. E. M. Siegbahn and R.-Z. Liao, *ACS Catal.*, 2020, **10**, 5603-5613.
330. P. E. M. Siegbahn, *RSC Adv.*, 2021, **11**, 3495-3508.
331. R. Breglia, C. Greco, P. Fantucci, L. De Gioia and M. Bruschi, *Inorg. Chem.*, 2019, **58**, 279-293.
332. S. Sicolo, M. Bruschi, L. Bertini, G. Zampella, G. Filippi, F. Arrigoni, L. De Gioia and C. Greco, *Int. J. Hydrogen Energy*, 2014, **39**, 18565-18573.
333. M. Bruschi, C. Greco, M. Kaukonen, P. Fantucci, U. Ryde and L. De Gioia, *Angew. Chem., Int. Ed.*, 2009, **48**, 3503-3506.
334. C. Greco, M. Bruschi, P. Fantucci, U. Ryde and L. De Gioia, *Chem. Eur. J.*, 2011, **17**, 1954-1965.
335. C. Greco, M. Bruschi, P. Fantucci, U. Ryde and L. De Gioia, *ChemPhysChem*, 2011, **12**, 3376-3382.
336. F. Arrigoni, L. Bertini, M. Bruschi, C. Greco, L. De Gioia and G. Zampella, *Chem. Eur. J.*, 2019, **25**, 1227-1241.
337. S. Sumner, P. Söderhjelm and U. Ryde, *J. Chem. Theory Comput.*, 2013, **9**, 4205-4214.
338. L. Hu, P. Söderhjelm and U. Ryde, *J. Chem. Theory Comput.*, 2011, **7**, 761-777.

This journal is © The Royal Society of Chemistry 20xx

Please do not adjust margins